Spring 1995

Effect of fiber-matrix coupling on the mechanical properties of a totally bioabsorbable composite

Barbaro Jesus Perez
New Jersey Institute of Technology

Copyright Warning & Restrictions

The copyright law of the United States (Title 17, United States Code) governs the making of photocopies or other reproductions of copyrighted material.

Under certain conditions specified in the law, libraries and archives are authorized to furnish a photocopy or other reproduction. One of these specified conditions is that the photocopy or reproduction is not to be "used for any purpose other than private study, scholarship, or research." If a, user makes a request for, or later uses, a photocopy or reproduction for purposes in excess of "fair use" that user may be liable for copyright infringement,

This institution reserves the right to refuse to accept a copying order if, in its judgment, fulfillment of the order would involve violation of copyright law.

Please Note: The author retains the copyright while the New Jersey Institute of Technology reserves the right to distribute this thesis or dissertation

Printing note: If you do not wish to print this page, then select "Pages from: first page # to: last page #" on the print dialog screen

ABSTRACT

EFFECT OF FIBER-MATRIX COUPLING ON THE MECHANICAL PROPERTIES OF A TOTALLY BIOABSORBABLE COMPOSITE

by
Barbaro Jesus Perez

The mechanical properties of a new class of bioabsorbable polymer-composite based on the amino acid tyrosine and calcium phosphate fibers were studied. The effect of the fiber aspect ratio on the elastic modulus of a discontinuous fiber composite was analyzed using the SMC composite micromechanics computer model. The mechanical stiffness of this polymer was found to be superior to that of poly-p-dioxanone, poly-ε-caprolactone and poly-o-ester.

The fiber surface was modified with methane plasma spray to improve the fiber-matrix coupling. The treated fiber composites had 16-40% higher tensile modulus than the untreated fiber composites. From the flexural test results it is suspected that the compression modulus is greater than tensile. The use of these innovative materials in fixation devices could eliminate a second surgery to retrieve the implant, eliminate the corrosion problems with metallic devices and provide load transfer to the healing bone, minimizing stress protection atrophy.

EFFECT OF FIBER-MATRIX COUPLING ON THE MECHANICAL PROPERTIES OF A TOTALLY BIOABSORBABLE COMPOSITE

by
Barbaro Jesus Perez

A Thesis
Submitted to the Faculty of
New Jersey Institute of Technology
in Partial Fulfillment of the Requirements for the Degree of
Masters of Science in Biomedical Engineering

Biomedical Engineering Committee

May 1995

APPROVAL PAGE

EFFECT OF FIBER-MATRIX COUPLING ON THE MECHANICAL PROPERTIES OF A TOTALLY BIOABSORBABLE COMPOSITE

Barbaro Jesus Perez

Dr. Clarence W. Mayott, Thesis Adviser — Date
Professor of Mechanical Engineering, NJIT

Dr. Harold Alexander, Committee Member & Immediate Supervisor — Date
Director of the Department of Bioengineering, Hospital for Joint Diseases
Orthopaedic Institute and Professor, Department of Orthopaedic Surgery,
New York University School of Medicine

Dr. Albert K. Narh, Committee Member — Date
Professor of Mechanical Engineering, NJIT

BIOGRAPHICAL SKETCH

Author: Barbaro Jesus Perez

Degree: Master of Science in Biomedical Engineering

Date: May 1995

Undergraduate and Graduate Education:

- Masters of Science in Biomedical Engineering,
  New Jersey Institute of Technology, Newark, NJ, 1995.

- Bachelor of Science in Mechanical Engineering,
  New Jersey Institute of Technology, Newark, NJ, 1992.

Major: Biomedical Engineering

Presentations and Publications:

Perez, Barbaro J., Harold Alexander and Clarence W. Mayott. "Mechanical Properties of a Discontinuous Random Fiber Composite for Totally Bioabsorbable Fracture Fixation Devices." *IEEE 21st Annual Northeast Bioengineering Conference Proceedings, University of Maine* (May 22, 1995).

Perez, Barbaro J., Harold Alexander and Clarence W. Mayott. "Mechanical Properties of a Discontinuous Random Fiber Composite for Totally Bioabsorbable Fracture Fixation Devices." *Fifth Annual Mini-Tech Student Conference (Best Paper Award in the Polymeric Materials Section), New Jersey Institute of Technology* (April 21 1995).

Perez, Barbaro J., Konstantin Caploon, and Christopher B. King. "ART" wheelchair patent disclosure filed with the New Jersey Institute of Technology (August 31, 1994).

This thesis is dedicated to my parents,
Jose and Lucia Perez, for all their love and support.

ACKNOWLEDGMENT

The author wishes to express his sincere gratitude to Dr. Harold Alexander and Dr. Clarence W. Mayott for their guidance, support and encouragement during the course of this research. Special thanks to Dr. Albert K. Narh for serving as member of the committee. Many thanks go to Dr. David Kristol and Sheridan Quarless for their support and excellent advice throughout the author's graduate education. The author also wishes to thank Jose Charvet, Lisa Anderson, Paul West and Dr. Deyu Chen from the Hospital for Joint Diseases (HJD) for their help with the manufacturing and mechanical testing and Dr. John L. Ricci (HJD) for his help with the SEM work. In addition, the help of Peggy Miller, Guo Gang Chen and Bill Green (HJD) is gratefully acknowledged.

The author is grateful to Dr. Joachim Kohn, Arthur Schwartz and Dr. Yuelie Lu (Department of Chemistry, Rutgers University, Piscataway, NJ) for supplying the DTE polymer, and performing the GPC analysis. The timely help of Dr. William C. LaCourse (New York State College of Ceramics, Alfred University, Alfred, NY) by supplying the CaP fibers and Dr. Ih-Houng Loh (Advanced Surface Technology, Inc., Billerica, MA) by performing the plasma treatment is sincerely appreciated.

The author wishes to acknowledge the technical support of Dr. George Brode (Integra Life Sciences, Inc.) and Dr. Mark Zimmerman (University of Medicine and Dentistry of New Jersey, Orthopaedic Department). In addition, Jack W. Gillespie, Jr. (Center for Composite Materials, University of Delaware) provided some of the literature and technical advise on the SMC software.

This work was partially funded by NIST-ATP Award 70NANB4H1502. Finally, the author wishes to thank the New Jersey Institute of Technology Graduate Studies Program for the graduate assistantship support provided throughout this work.

TABLE OF CONTENTS

TABLE OF CONTENTS
(Continued)

LIST OF TABLES

LIST OF TABLES
(Continued)

LIST OF FIGURES

LIST OF FIGURES
(Continued)

Figure **Page**

LIST OF FIGURES
(Continued)

Figure **Page**

CHAPTER 1

INTRODUCTION

1.1 Anatomy and Physiology of Bone

Bone is a complex tissue which can be thought of as having several levels of structure. It is a highly specialized form of connective tissue composed of bone cells in an extracellular composite material [1]. At its most fundamental level, hydroxyapatite (HA) crystals, $Ca_{10}(PO_4)_6(OH)_2$, are embedded between collagen fibrils [2]. The HA mineral provides rigidity, while the collagen provides some ductility. The synergistic effect for bone is that it absorbs greater energy before failure as well as permitting high load bearing and stiffness [3].

At the second level, collagen and HA fibrils configure themselves into sheets (lamellae) with a preferred direction. Similarly to laminated composites, the orientation of these sheets define the directions of maximum and minimum strengths for a primary loading direction. The third structural level is the arrangement of these lamellae. Lamellae may arrange themselves into sheets, or circular concentric structures such as a tubular Haversian osteon [3].

The fourth level of structure represents the fundamental macroscopic types of bone, cortical and trabecular. At this level density is the controlling factor governing the strength. Trabecular orientation is also important in defining the maximum and minimum strength directions [3]. Compact or cortical bone is hard and dense and forms the outer shell of bones; it consists of bony tissue arranged in concentric layers (Haversian systems) [2]. Trabecular bone (cancellous), also know as "spongy bone," is located in the intramedullary zone and consists of a loose network of rigid beams (trabeculae) [4]. The relative quantities of these structures depend on the function of the specific bone.

Bone is a living tissue, thus it must be provided with an adequate supply of nutrients; the Haversian system serves that purpose. The Haversian system consists of a central hole (Haversian canal) surrounded by rings of lamellae. The bone cells or osteocytes, reside between the lamellae in spaces called lacunae. Tiny pores (canaliculi) connect the osteocytes with one another and with the Haversian canals. The blood flows through the Haversian canals and canaliculi to supply the osteocytes with oxygen and nutrients and to remove the waste products [4]. This osteo-vascular system is especially important in fracture healing [5].

There are three types of bones cells: osteoblasts, osteocytes, and osteoclasts. Osteoblasts form bone via the secretion of collagen which then becomes mineralized. Once surrounded by calcified matrix, the osteoblasts become osteocytes. Osteocytes play a key role in the dissolution of bone mineral for the homeostatic regulation of calcium in body fluids [2]. Osteoclasts are large multinucleated cells that break down (resorb) previously formed bone.

1.2 Biological Mechanisms of Fracture Repair

There are three biological stages of fracture repair: inflammatory, reparative, and remodeling [6]. During the inflammatory stage a hematoma accumulates within the medullary canal in the endosteum and beneath the periosteum (a fibrous membrane covering the bone). Both periosteum and endosteum have osteogenic (bone forming) potential. The bone within the fracture region becomes necrotic due to lack of blood supply, creating an inflammatory response with macrophage invasion to digest the debris.

The reparative stage begins within two to three days after injury, as the hematoma becomes organized. This is evident with the formation of fibrous tissue, fibrocartilage and hyaline cartilage [6]. These materials seal the fragment ends together. New bone is formed underneath the periosteum around the ends of the fracture and grows toward the fracture site. A similar process transpires at the endosteum. The cartilage tissue is then

replaced by bone. This is what is known as secondary ossification because the ossification occurs after the initial callus formation. Primary ossification is the fusion of fractured bone ends without callus formation [1].

The final stage of fracture healing occurs over a long period of time. Bone remodeling, performed by osteoclasts and osteoblasts, removes the superfluous tissue around the fracture site until bone returns to its original shape [6]. Bone remodeling is a phenomena by which bone adjusts its size and shape in the most efficient manner to support a specific loading condition.

1.3 Biomechanics of Fracture Fixation

One of the important factors in achieving primary ossification of the fracture site is the prevention of micromotion of the bone ends. Motion of these ends will stimulate callus formation and secondary healing will occur. In the worst case, excessive motion could even prevent secondary ossification and cause a non-union [1].

As the fracture site undergoes the stages of healing the biomechanical properties of the bone change. There are significant increases in maximum torque to failure and energy absorption throughout the healing process [7]. This is attributed to the increase in cross-sectional area of new bone in the healing region as a result of the callus formation. The increase in area is of most benefit if the new bone is deposited as far away from the central axis as possible, since this increases the bone's moment of inertia and in turn its stiffness and strength.

The change in material properties in the vicinity of the fracture site also plays an important role. A decrease in bone porosity as the trabecular structure matures and an increase in the mineral content of the healing tissue are responsible for improvements in material properties [8]. In addition, total re-vascularization of the healing site seems to restore the biomechanical properties of the bone nearly back to normal [9].

1.4 Fracture Fixation Devices

1.4.1 History of Bone Plates

Currently orthopedic surgeons have several fracture fixation methods at their disposal for the immobilization and treatment of fractured limbs: internal and external or closed treatments. Closed methods refers to casting and external immobilization of the injured site, while open methods require surgical intervention and the introduction of an implant. Internal fracture fixation devices include: bone plates, intra-medullary (IM) nails, pins and K-wires. The bioabsorbable material discussed in this thesis are meant to be used to fabricate bone plates, pins and IM-nails for the fracture management of low load bearing bones. Only bone plates will be discussed here, since they are probably the oldest and would be good first candidates for these materials.

The use of bone plates was first reported in 1886 [10], although earlier use can't be ruled out since during the American Civil War several metal devices were used experimentally. The primary concern of early researchers was infection prevention, device strength and tissue tolerance [1].

In 1949, the effects of compressive forces on bone plates was first addressed [11] [12]. These investigators believed that the compressive forces, which pushed the newly fractured ends of bone together, would produce more rapid bone growth. Around 1958 a self-compressing plate was developed by G. W. Bagby and J. M. Janes [13]. The screws had a conical shoulder which glided down the edge of an oval screw hole and compression was achieved as the screws were driven home. This design was very successful in a canine femoral osteotomy model and in later clinical trials [14] [15].

There was some controversy regarding the actual effect of compressive forces on healing bone. Some researchers found no significant differences in using compressive plates [1]. Since then, it is generally accepted that even though compression itself does not stimulate bone growth, the opposition of the bone ends due to compression is crucial

if rapid primary bony union is to occur [16]. In fact, most of today's bone plates are of the compressive type.

1.4.2 Biomechanical Requirements of Bone Plates

The three main purposes of an artificial bone plate are: buttressing, neutralization and compression of the fracture site. The static compression of the bone fragments provides interfragmentary friction to oppose shearing forces which would otherwise induce large bending moments and torque on the plate. If compression is not applied, motion between the fragments can occur. The motion can stimulate bone resorption at the opposing ends of the fragments creating instability.

The elastic modulus of cortical bone ranges from 17 to 24 GPa depending upon age and location of the specimen [3]. The modulus of elasticity increases from birth until age 50 and then starts to gradually decrease. Bone is strongest in longitudinal compression loading (ultimate strength $\approx$ 190 MPa) followed by longitudinal tension (ultimate strength $\approx$ 130 MPa) [3].

Bone plates are usually exposed to bending forces in vivo. They undergo high cyclic bending stresses and lesser torsional moments. This requires adequate inplane and shear properties [17]. Lawrence, et. al. [18] have measured the bending moment on a single bone plate, offset by 2 cm from the line of action in the tibia of a 67 kg person, during a normal gait cycle to be 54 Nm. The torsional moment measured ranged from 13.7 Nm to 18.4 Nm . Other workers have done similar measurements on cadaver femurs with several types of metal plates and found that the bending moment ranged between 44 Nm and 66 Nm [17]. The bending moment to failure and maximum bending stiffness to produce pain in humans has been observed to be 25-30 Nm and 2.0 Nm/degree, respectively [19].

Studies indicate that rigid fixation (about 60% of intact bone bending stiffness) with a small fracture gap produces primary ossification with little callus formation, while more flexible fixation (about 20% of intact bone bending stiffness) with a larger fracture gap produces more callus [3]. Experiments have demonstrated that repetitive loading is a key factor in stimulating new bone formation, as compared with static compression [20].

1.4.3 Problems with Metal Bone Plates

The most commonly used bone plates today are made of metal (stainless steel and titanium alloys) [1]. Steel has an elastic modulus approximately ten times that of cortical bone (316L steel $\approx$ 210 GPa, cortical bone $\approx$ 18 GPa). The rigidity of steel plates can be an advantage during the early healing period, but the same rigidity can be a strong disadvantage later. Investigators in the field have discovered that rigid fixation leads to bone remodeling and ultimately osteoporosis and atrophy due the stress protection produced by the plates [19] [21-23].

Bone plates shift the neutral axis away from the centroidal axis of the bone. This shifts the stress distribution towards the plate, changing the amount of load the bone experiences. If the plate is not removed once the fracture has healed, it can continue to carry the majority of the load and therefore understrain the bone beneath, leading to osteoporosis and eventually atrophy. If the removal of the plate becomes necessary at a later date, the remaining bone may not be sufficiently strong to support loads and a refracture of the bone may occur [3].

Another problem associated with metal plates is corrosion. Any form of corrosion can lead to premature cracking due to stress and fatigue of the implant [1]. Corrosion products are also a serious biocompatability concern. Chromium, cobalt, iron, nickel and titanium have been linked to carcinogenic effects in animal and human studies [24] [25].

1.5 Bioabsorbable Materials

Due to certain disadvantages of metallic devices, other types of materials such as polymers, ceramics and composites have been studied. Composites particularly offer attractive features such as stiffness variation by manipulation of fiber volume and orientation. Some of these composites include: glass/epoxy, graphite/polysulfone and graphite/polypropylene systems. Bone plates fabricated from these non-degradable materials had lower flexural rigidity than conventional plates and did in fact provide less stress shielding than their metallic counterparts [26]. Some degree of stress protection atrophy still occurred.

The ideal bone plate would lose its stiffness at a rate corresponding to the gain in structural properties of the healing fracture, thus allowing progressive load sharing, while maintaining the stiffness of the fixation/bone construct [27]. This is where the biodegradable materials open a new door of opportunities. Another added benefit of biodegradable materials is that retrieval operations for device removal would have to be undertaken only to address cases of device failure, non-union or infection. This would mean a decrease in the risks to the patient associated with general anesthesia and also a savings to the health care system.

Due to the stringent requirements that absorbable materials must meet, the list of candidates quickly shortens. The most widely used materials for absorbable orthopaedic implants are those which were initially developed for absorbable sutures [28]. These are α-polyesters: polyglycolic acid (PGA), polylactic acid (PLA) and polyparadioxanone (PDS). PGA was first developed by the American Cyanamid Co. in 1962 under the trade name of Dexon®. Copolymers of PGA/PLA have also been commercialized as absorbable Vicryl® sutures. There are other bioabsorbable materials available that are less widely known, including: poly-β-hydroxybutyrate (PHB), poly-β-hydroxyvalerate (PHV), poly-ε-caprolactone (PCL), polyorthoester (POE) and the new tyrosine derived polycarbonates [28] [29].

The degradation mechanism of these materials is mainly by hydrolysis, although enzymatic activity in vivo does increase the degradation process [30]. Water first diffuses into the material and causes swelling due to the disruption of intermolecular bonding within the material. In PGA, PDS and PLA, water is believed to cleave covalent bonds of the polyester groups within the polymer chains leading to chain breakdown and molecular weight degradation. Mass and strength loss eventually follows.

Some of the first uses of these materials for fracture fixation devices were conducted in 1971 by investigators who used PLA rods, screws and plates to treat mandibular fractures in dogs [31] [32]. These studies showed the lack of strength of these materials and the need for an absorbable reinforced composite. This led to the development of self reinforced (SR) materials such as BioFix® (PGA) and oriented materials such as Orthosorb® (PDS), which are currently available commercially as pins for cancellous bone fixation [28]. There are however, some biocompatability concerns with these materials. A recent study of 516 patients who were treated with SRPGA rods revealed complication rates of 1.2% for failure of fixation necessitating reoperation, 1.7% for bacterial infection of the wound, and 7.9% for late noninfectious inflammatory tissue response that warranted operative drainage [33].

Other researchers developed fixation devices using high strength carbon fibers in a PLA matrix [1] [27]. The carbon fibers have been found to provide a scaffold for tissue ingrowth and increase the stiffness and strength of the polymer matrix. These works supported the concept of low modulus plating and introduced the idea of using a partially absorbable composite material. A concern with the PLA system was the delamination of the composite plates due to water absorption leading to hypertrophic nonunions. Other studies of the PLA material indicate late inflammatory foreign-body reactions and increased osteoclastic activity [34] [35]. The lactic-acid-rich degradation products have the potential to significantly lower the local pH in a closed space surrounded by bone. It

is hypothesized that this acidity tends to cause abnormal bone resorption and/or demineralization which could lead to a cytotoxic environment [35].

1.5.1 Tyrosine Polycarbonates

Recently a new class of bioabsorbable materials was developed by Kohn, et. al. [36]. The synthesis of these new materials was based on derivatives of the naturally occurring amino acid L-tyrosine. Tyrosine-derived dipeptides replaced the diphenols employed in the synthesis of commercial polycarbonates. The length of the pendant chain (Fig. 1) can be modified by these dipeptides (ethyl, butyl, hexyl and octyl esters of desaminotyrosyl) to influence important polymer engineering properties.

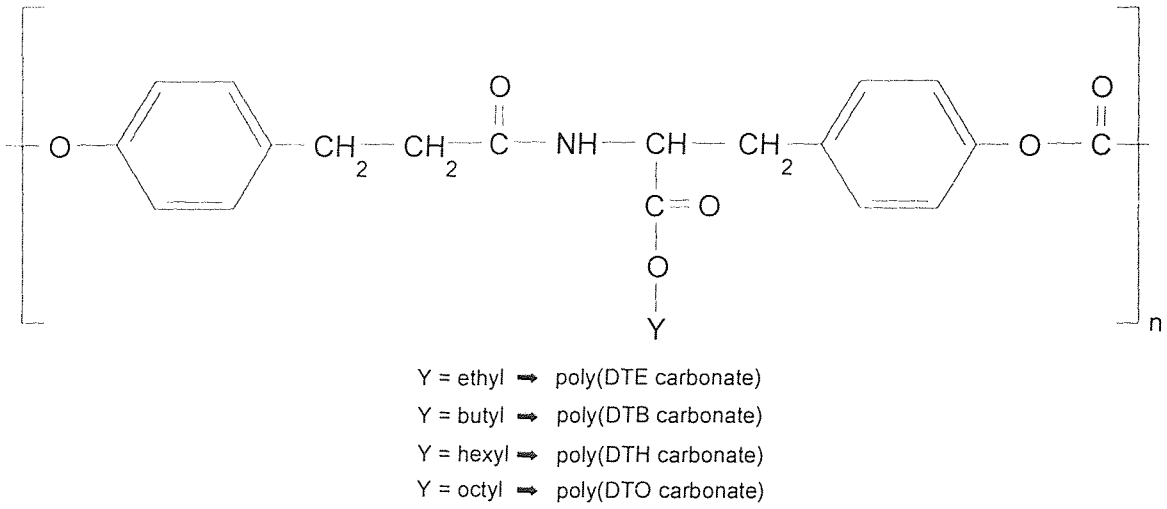

Figure 1 Tyrosine-derived polycarbonates [36].

Tyrosine-derived polycarbonates appear to be promising materials for orthopaedic applications. A recent comparative study with PDS-based Orthosorb® pins indicated that these new materials were mechanically stronger and degraded slower than PDS [37]. This could be beneficial in cases where more support is needed or slower healing is expected. Another interesting characteristic of these materials is their bone ingrowth potential. In the same study, significant bone ingrowth into the tyrosine-derived

polycarbonate pins was observed as early as one week after implantation. After four weeks, the trabecular network inside the pins was denser. This is very encouraging since it may provide strong implant anchorage and stimulate the progressive transfer of stress to the newly formed bone.

The initial tensile modulus of these materials was found to range from 1.2-1.6 GPa [38]. Tyrosine-derived polycarbonates are stiffer than many degradable polymers, including PCL, POE and PDS which have an elastic modulus of 0.5 GPa, < 1 GPa and 0.94 GPa, respectively, but are not as stiff as PLA and PGA which have an elastic modulus of 5 GPa and 6.5 GPa, respectively [1] [39]. The DTE and DTB polycarbonates had a tensile failure strength at break of 67 and 60 MPa and failed without yielding after 4% elongation, while the DTH and DTO were ductile, yielding at 5% elongation with a yield point of 62 and 51 MPa, respectively. The weight average molecular weights of the polymers ranged from 120,000-450,000 da [38] prior to degradation.

The degradation mechanism seems to involve the rapid cleavage of the pendent chain ester bonds followed by a slower hydrolysis of the carbonate bonds [38]. In vitro degradation proceeded at a similar rate as in soft tissue while an accelerated process occurred in hard tissue [37]. The length of the pendent chain affected the degradation behavior and strength retention; the polymers with short pendent chains were more readily hydrolyzable [38].

In vitro cytotoxicity studies have also been conducted. The tyrosine-derived polycarbonates did not elicit any noticeable cytotoxic effect on fibroblast cells, except for the more hydrophobic poly(DTO carbonate) which caused patchy cell death [36]. Cell proliferation was modulated by the pendent chain length; the least hydrophobic polycarbonate (DTE) being a more stimulating substrate for cell growth than the more hydrophobic polymers. This thesis will focus on poly-(desamino-tyrosyl-tyrosine ethyl ester) (DTE).

1.5.2 Calcium Phosphate Fibers

Historically, the use of ceramic materials in orthopedic surgery dates back to 1892 when plaster of Paris (calcium sulfate) was used as a bone substitute [40]. Ceramic materials are extremely inert since they are fully oxidized, thus eliminating the possibility of corrosion [1]. Ceramics can be fabricated with a porous structure to allow tissue ingrowth and provide a scaffold for bone growth and attachment [3]. These materials have been used as bone defect fillers in the following forms: calcium sulfate ($CaSO_4$), calcium phosphate (CaP), calcium oxide (CaO) and aluminate (Al_2O_3), β-tricalcium phosphate ($Ca_3(PO_4)_2$) and hydroxyapatite [1]. Calcium sulfate has also been used for the short term delivery of antibiotics and bone morphogenic proteins [41] [42].

Ceramic materials can also be manufactured as glasses. Ceramic glasses are of particular interest since they offer better mechanical properties and thus could be potential absorbable reinforcements [43-45]. Calcium phosphate glass fibers have been fabricated using various composition of Ca, ZnO, Fe_2O_3, P_2O_5, and Na. These CaP glass fibers can be degraded by water in an in vivo environment. Hydrolysis can occur at the P-O-P bonds producing P-OH end groups which are susceptible to acid/base reactions [1]. Water can also hydrate the entire chain; this is when the water "wicks-down" the entire fiber length.

The fairly rapid degradation process must be slowed down in order to retain the mechanical properties of composite fracture fixation devices for the required time. Using a hydrophobic matrix to protect the fibers can decrease the degradation rate. Also the use of short fibers instead of continuous fibers, slows down the "wicking effect" since the water must now pass through more matrix to hydrolyze all of the fibers. Surface modification of the fibers through plasma treatment have been also found to retard the degradation process [46] [47].

CHAPTER 2

MATERIALS AND METHODS

2.1 Analytical Calculations of Composite Materials

2.1.1 Introduction

A useful definition of a composite is, "the combination of a reinforcement material (such as a particle or fiber) in a matrix or binder material" [48]. The term composite implies that the component materials are macroscopically identifiable. The advantage of a composite material is that it usually exhibits a synergistic effect of some of the constituent's properties. The following are other major advantages that composites have over competitive materials (usually metals):

- High specific tensile strength (ratio of material strength to density)
- High specific modulus
- Improved fatigue life
- Corrosion resistance

Some of the major disadvantages are;

- High cost of manufacturing
- Complexity of material behavior (synergy of undesirable material properties)
- Increased sensitivity to the environment (temperature, moisture and chemical agents)

There are three general types of composites: laminated, fibrous and particulate [49]. This work will be limited to discontinuous fibrous composites. These types of materials have been widely used in the automobile, aircraft, medical, and sports

equipment industry in products such as car panels, airplane struts, medical prostheses and ski equipment [48]. The analysis of such products is well documented in many works [49-52].

Composites material properties are described from two points of view, micromechanics and macromechanics. Micromechanics is the study of composite material behavior wherein the interaction of the constituents is examined at the local level. Macromechanics is the study of composite material behavior where the material is presumed homogenous and the effects of the constituents are detected only as averaged apparent properties of the composite [1].

2.1.2 Micromechanics of Chopped Fiber Composites Using SMC

A discontinuous fiber composite consists of chopped fibers imbedded in a polymer matrix. The fibers serve as the reinforcement while the matrix supports and protects the fibers. In addition, the matrix, transfers the load to the fibers through shearing stresses.

Aligned continuous fiber composites have microstructures which allow the implementation of mathematical simplifications to produce reasonable estimates of their elastic behavior. Some of these estimates (elastic modulus) can be obtained through the well known "rule of mixtures." However, the situation for chopped fiber composites is much more complex. This complexity is reflected through variable states of fiber orientation and distributions of fiber lengths coupled with dispersed or aggregate textures [53].

The SMC (Sheet Molding Composites) micromechanics model for composite materials, a computer program developed by the University of Delaware Center for Composite Materials, was used to predict the elastic properties of the DTE/CaP discontinuous fiber composites. This software package can predict the thermoelastic properties of a wide range of composite materials (continuous fiber lamina, particulate reinforced composites, porous composites and foams, chopped fiber sheet molding

materials, short-fiber bulk molding materials, and circular platelet reinforced composites) [54]. Not all of the equations for the calculations made by this program will be discussed in this paper. The theoretical basis for these calculations can be found in the following references: [53] and [55-59].

Microstructural parameters such as composition, degree of orientation of the reinforcement and constituent properties are the program's input parameters. The following are the basic assumptions of the micromechanics model used by SMC [54]:

1. Perfect bonding (Chemical and/or physical) between the fiber and matrix.
2. Statistical homogeneity. Significant variations in the reinforcement distribution and orientation within the composite structure are common in short fiber composites. This represents, the most common source of discrepancy between predicted and observed properties.
3. The distribution of fiber aspect ratios (length/diameter) falls within a narrow band about an average value. A broad distribution may result in deviations between the predicted and observed properties.
4. The fiber orientation distributions are assumed to be uni-modal, centered about the origin of the principal axes.
5. The matrix and reinforcement materials are assumed to be isotropic.

In discontinuous fiber composites, the fiber length will have a dramatic effect on the elastic properties of the material. An imposed load is transferred to the fiber by matrix shear stresses acting over the surface of the fiber. The section of the fibers near the ends is referred to as the "ineffective" or "critical" length (L_c) and is defined as the length required for the stress to achieve 95% of the asymptotic value experienced by the matrix at a point far away from the fiber. The critical aspect ratio for a cylindrical fiber is defined as L_c/fiber diameter. In order for the fiber to provide significant reinforcement,

the fiber aspect ratio must be greater than the critical aspect ratio [53]. The range of aspect ratio for short fiber reinforcements is between 1 and 1,000 [54]. The aspect ratio may be the most dominant geometric parameter governing the elastic behavior of a chopped fiber composite [53].

In general, individual fibers will be oriented in 3-dimensions. Three Eulerian angles are required to define their orientation as illustrated in Fig. 2. The angle ϕ measures the orientation of fiber projections within the "1-2" plane with respect to the longitudinal 1-axis. The angle θ quantifies the degree of tilt out of the "1-2" plane for individual fibers. The angle ψ is redundant for ellipsoidal particles (SMC assumes ellipsoidal inclusions) and is not required for input into the program [54].

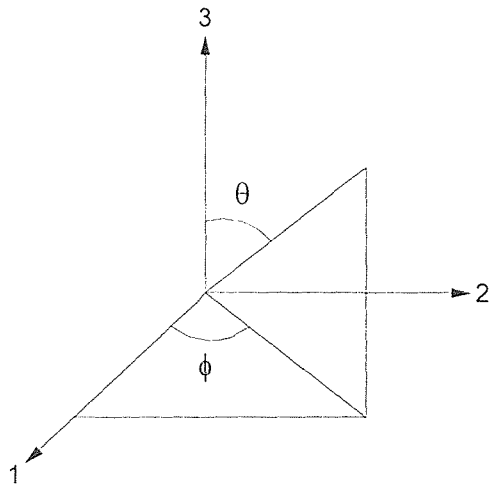

Figure 2 Three dimensional fiber orientation definition via Eulerian angles [54].

The following equations, taken from references [53] and [54], describe the derivation of the cosine fiber orientation distribution used by SMC:

$$\int_0^{\pi}\int_0^{\pi/2} N(\phi,\theta)\sin\theta d\phi d\theta = 1 \qquad (1)$$

where,

$N(\phi, \theta)$ = distribution function which defines the fraction of fibers that share a common orientation.

The following symmetry conditions are required:

$$N(\phi,\theta) = N(-\phi,\theta) \tag{2}$$

$$N(\phi,\theta) = N(\pi+\phi,\theta) \tag{3}$$

$$N(\phi,\theta) = N(\phi,-\theta) \tag{4}$$

Assuming that the orientation distribution is separable,

$$N(\phi,\theta) = N_p(\phi)N_a(\theta) \tag{5}$$

where,

N_p = planar distribution
N_a = axial distribution

and satisfies the normalization conditions,

$$\int_0^{\pi} N_p(\phi)d\phi = 1 \tag{6}$$

$$\int_0^{\pi/2} N_a(\theta)\sin\theta d\theta = 1 \tag{7}$$

then

$$N_p(\phi) = A_p \cos^{k_p}\phi \tag{8}$$

$$N_a(\theta) = A_a \cos^{k_a}\theta \tag{9}$$

where,

A_p = planar orientation averaging tensor
A_a = axial orientation averaging tensor

Finally, vector and tensorial averages (see reference [53] for complete derivation) along with the simplifications in equations (5), (8) and (9) result in only two independent orientation parameters being required to specify the general state of fiber orientation.

Defining

$$< \cos^2 \phi > = \int_0^{\pi} N_p(\phi) \cos^2 \phi \, d\phi \tag{10}$$

$$< \cos^2 \theta > = \int_0^{\pi/2} N_a(\theta) \sin\theta \cos^2\phi \, d\theta \tag{11}$$

then

$$f_p = 2 < \cos^2 \phi > -1 \tag{12}$$

$$f_a = \frac{1}{2}[3 < \cos^2 \phi > -1] \tag{12}$$

where,

f_p = planar orientation in the "1-2" plane (Fig. 1)

f_a = axial orientation about the "3" or perpendicular plane (Fig. 1)

The values of f_p range from zero to one. Values of zero correspond to a random distribution in the "1-2" plane. When f_p = 1 the fibers are totally aligned to the 1-axis in Fig. 1. The values of f_a range from -0.5 to +1.0 and measure the tendency for fibers to tilt out of the "1-2" plane and align parallel to the normal 3 direction. For f_a = -0.5, all the fibers lie perpendicular to the 3-axis, f_a = 0 corresponds to a random distribution in the angle θ, and f_a = 1 implies that all fibers are aligned along the 3-axis [54].

A random-planar fiber orientation was assumed for the DTE/CaP composites due to the small sheet thickness. This assumes that the fibers are confined to lie in the "1-2" plane with minimal out-of-plane tilting. The assignment of f_a = -0.5 assures that the fibers are confined to the "1-2" plane while f_p = 0 yields random fiber orientation in the "1-2" plane [54].

The SMC software requires the user to enter mechanical properties for both the fiber and polymer material. The DTE elastic modulus entered was the mean value obtained from the tensile test. Poisson's ratios of 0.33 (from industrial grade polycarbonate) and 0.22 (from E-glass fibers) were used for the polycarbonate DTE and the CaP fibers, respectively [53]. The SMC program outputs the thermoelastic properties of the mentioned composite systems for various fiber volumes, aspect ratios and orientations.

2.2 Fabrication Processes

2.2.1 Introduction

One of the major differences in designing with polymeric materials versus metals is that the fabrication parameters can have a significant impact on the mechanical properties of the product. This is why careful planning of the manufacturing processes must be made at the start of any new plastic design project. DTE like any new polymer, is no exception. Along with choosing the correct processing parameters such as temperature, pressure and cooling rate manufacturing costs must be minimized if the product is going to be competitive in today's markets.

Injection molding is the most widely used process for high-volume production of thermoplastic resin parts, reinforced or otherwise [60]. Pellets of resin with or without fiber reinforcement are fed into a hopper and then into a heated barrel containing a rotating screw that mixes and heats the material. The heated resin is then forced at high

pressure through sprues and runners into a matched-metal mold. Molding is rapid, and parts can be very precise and complex. This process however, usually requires a large amount of polymer, making it inappropriate to investigate the fabrication parameters of a new material such as DTE.

Compression molding is one of the least expensive plastic forming processes. It offers more control over the dimensional accuracy of the product, as the entire part surface is in contact with the mold. Machining can be virtually eliminated since holes and slots could be molded into the part. However, compression molding does have its disadvantages, flow patterns within the dies can result in weaknesses at knit (weld) lines, where different streams of compound flow together in the mold and certain shapes can result in voids or incomplete mold filling [61].

The two processes mentioned above are probably the most widely used in the composite industry today. There are other fabrication techniques which are also employed. Some of these include: filament winding, braiding, hand lay-up and pultrusion. This paper will concentrate on the compression molding process, but the following references are included for further reading on this subject [62-66].

2.2.2 "Neat" DTE Polymer Sheet Fabrication

The DTE polycarbonate was obtained from Dr. Joachim Kohn (Dept. of Chemistry, Rutgers University, Piscataway, New Jersey). The method of polymerization used was a phosgenation/capping reaction followed by direct isopropyl alcohol precipitation of the desamino-tyrosyl-tyrosine ethyl ester. The low molecular weight grade was end-capped and had a tan powdery particulate appearance. Table 1 lists DTE's physical properties.

Table 1 Poly(DTE Carbonate) properties of Batch # ALS 011995.

Weight Average Molecular Weight, M_W (da)	68,000
Number Average Molecular Weight, M_n (da)	31,000
Glass Transition Temperature (°C)	93
Decomposition Temperature[a] (°C)	290
Density[b] (g/cm^3)	≈ 1.2

a - Obtained from reference [38]
b - Measured experimentally by author

The molecular weight measurements were obtained, prior to processing, via gel permeation chromatography (GPC) at a rate of 1 ml/min, using tetrahydrofuran (THF) as the solvent medium. The "neat" DTE (polymer alone) was molded into 40-mm^2 sheets, approximately 0.5 mm thick using a Carver Laboratory Press (Model C). The hydraulic press is equipped with top and bottom electric heaters and water heat-exchangers. A frame-type mold, with a 1.4-cm^3 cavity volume, was used (Fig. 3). The mold temperature was monitored via a thermocouple located in the center of the frame. The polymer was introduced between two thin Teflon sheets (0.01-mm thick) to prevent it from sticking to the mold surfaces. The mold was then introduced between the press plates and kept under slight pressure until the temperature reached 116 °C. At this point in time, a constant pressure of 40.6 MPa was applied for 5 minutes. The maximum temperature allowed was 127 °C. The mold was then cooled to room temperature at a rate of approximately 30 °/min. Finally, the mold was disassembled and the polymer sheet removed. These techniques and processing parameters were found to be optimum to completely fill the mold cavity, prevent sticking of the sheet to the mold surfaces and minimize polymer degradation. They were arrived at through experimentation and the previous work of Lisa Anderson (Duke University, North Carolina) during her NSF Scholar Internship at the Hospital for Joint Diseases.

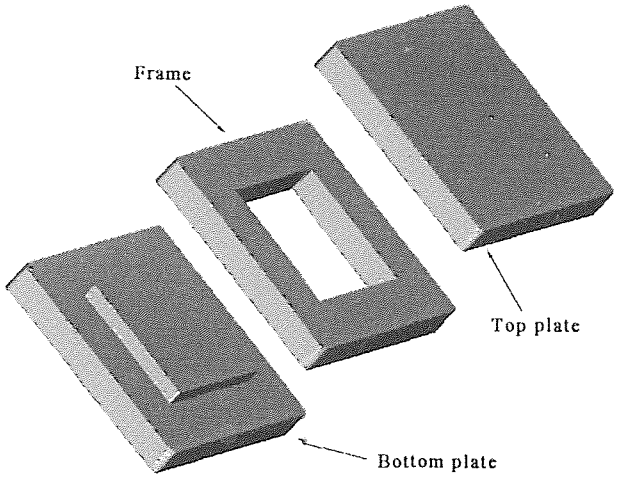

Figure 3 Frame-type mold used for compression molding.

2.2.3 Calcium Phosphate Fiber Fabrication

The CaP glass fibers were obtained from Prof. William C. LaCourse (New York State College of Ceramics, Alfred University, Alfred, New York). The fibers were composed of 27% Ca, 12% ZnO, 4.5% Fe_2O_3, 54% P_2O_5, and 2.5% Na and were drawn from a molten glass fired at 800 °C through a platinum bushing and were wound onto a cylindrical mandrel spinning at about 1,200 r.p.m [43]. The wound fibers were cut into 300 mm long strands. Some of the physical and mechanical properties of the CaP fibers are listed in Table 2.

Table 2 Calcium phosphate fiber properties [43].

Nominal Fiber diameter (μm)	20
Ultimate Tensile Strength (MPa)	700
Modulus of Elasticity, E (GPa)	50
Melting Temperature (°C)	759
Density (g/cm^3)	2.86

2.2.4 Fiber Surface Treatment

The CaP fibers were sent to Advanced Surface Technology (AST), Inc., Billerica, Massachusetts for surface plasma treatment. Dr. Ih-Houng Loh, of AST, modified the fiber surface using methane (CH_4) gas plasma treatment. The experimental apparatus used for plasma surface modification consisted of a quartz reactor chamber, a radio frequency generator, a gas inlet system and controls, and a vacuum pump and control system.

The fiber bundles were mounted on a glass rack, which was then positioned in the center of the plasma chamber. The pressure of this chamber was reduced below 0.1 mmHg. The reacting gas (CH_4) monomer was introduced and allowed to flow for approximately 10 min before turning on the plasma. The chamber pressure was maintained at 50 mmHg throughout the reaction period. The plasma was generated using a radio frequency generator operating at 13.56 MHz. The power was generally between 50-100 W. The thickness and surface energy on the substrates and the concentration of gas monomers in the reacting vapor determined the reaction time [46]. For a 10^3 Å thickness the reaction lasted approximately 10 min . The plasma was then turned off and inert gas (helium) was used to bring the system back to atmospheric pressure. Helium after treatment prevents oxidation of the fiber surface [47]. The fibers were removed and vacuum sealed for shipment.

2.2.5 Chopped Fiber Composite Sheet Fabrication

The chopped random planar fiber composite sheets (20%, 30%, 40% fiber by volume) were fabricated via a prepreg method. The CaP fibers were chopped, using an electric razor, to lengths of 2-4 mm. A weighed amount of chopped fibers (0.56, 0.85, 1.13 gms for 20, 30 and 40% fiber, respectively) was placed randomly in a 40-mm^2 aluminum foil cavity.

The DTE polymer (0.96, 0.84, 0.72 gms for 20, 30 and 40% fiber, respectively) was dissolved in 5.5-mL of methylene chloride, using a Vortex shaker, and poured into the cavity containing the chopped fibers. The prepreg was dried for at least 3 days in a vacuum dessicator before further processing.

The prepregs were molded into 40-mm^2 sheets approximately 0.5-mm thick using a Carver Laboratory Press (Model C). Teflon sheeting (0.01-mm thick) was used between the mold surfaces to avoid sticking. The temperature at the time of compression was 116 °C. The temperature was not allowed to exceed 127 °C. A constant pressure of 40 MPa was held for 5 min. The mold was then cooled to room temperature at a rate of 30 °/min. The Teflon sheets were removed from the composite sheet.

2.2.6 Preparation of Specimens for Mechanical Testing

Both tensile and flexural specimens were cut slightly over sized using a surgical scalpel. The samples were sanded down to 40 × 5 mm using #240 and then #600 grit carburundum paper. The samples were carefully screened for signs of stress concentrations and cracks. All samples were measured with digital calipers. The mean width and thickness of each sample were obtained from three measurements.

Cellulose triacetate tabs were glued on with cyanocrylate to protect the tensile test specimens from grip damage and reduce stress concentrations. The tabs were sanded in a ±45° fashion to prevent grip slippage. A 20-mm gauge length was used (Fig. 4). Each specimen was numbered appropriately for tracking purposes.

The flexural test specimens did not required any tab material. They were marked for proper alignment in the testing fixture, and numbered for tracking purposes. A 30-mm beam span was used, giving a 60 span/thickness (L/h) ratio. The literature suggest a L/h ratio of at least 32 in order to minimize the influence of interlaminar shear deformation and to achieve failure in bending rather than in interlaminar shear. In fact, if

the specimens are not strained gauged and only deflection is measured, higher L/h ratios are desirable [67].

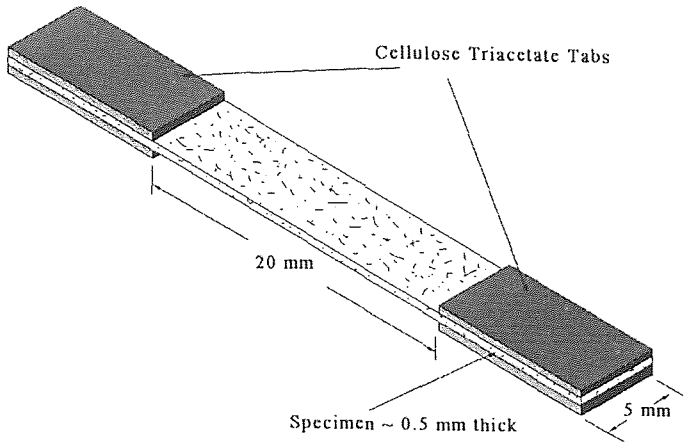

Figure 4 Tensile test specimen.

2.3 Mechanical Testing

2.3.1 Tensile Test

The tensile test was based on ASTM D638 and ASTM D3039-76 for the neat polymer and composite, respectively. However, the specimen dimensions were changed from the recommended value due to the smaller mold available. All tensile tests were carried out on an Instron Uniaxial Testing Apparatus (Model 1321). A 10 kN load cell was used to measure the load. The specimens were held with pneumatic grips and pulled at a cross-head speed of 0.2 mm/min until failure.

The data acquisition was performed using LabTech data collection software on an IBM compatible 386 PC. A 1 Hz sampling rate was used to collect the data. An Omega X-Y-T chart recorder (Model Omegaline 1321) was used as a backup recording system. Load and stroke data were collected and exported to a spreadsheet, containing specific specimen information such as width and thickness, to obtain the modulus via a least-squares curve-fit method. The spreadsheet was used to calculate the stress and strain at

failure for each specimen as well. Care was taken to protect the failure site of each specimen by securing them with tape in individual containers.

2.3.2 Flexural Test (Three Point Bending)

The flexural test was based on ASTM D790-1. Once again, the specimen size was changed from the recommended, because of the mold cavity constraint. Due to the small specimen size, a three point bending test was chosen instead of a four point bending test. The same testing apparatus and data collection setup as in the tensile tests were used. However, a 500 N load cell was installed to accurately measure the smaller loads and data were sampled at 5 Hz.

An aluminum three point bending testing fixture was built (Fig. 5) with supports (stainless steel dowel pins, 3.175 mm in diameter) set 30 mm apart. A maximum deflection of 6 mm (≈ 2.2% strain) and 7 mm (≈ 2.8% strain) was used for the neat DTE and composites, respectively with a cross-head speed of 5 mm/min. The spreadsheet calculated the flexural modulus and stress and strain to failure when possible. Some samples did not break. All failed specimens were also secured and saved for SEM analysis.

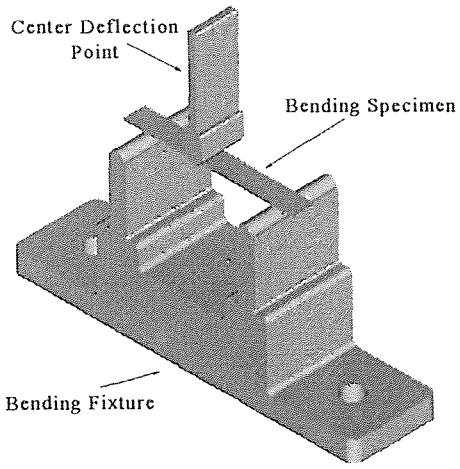

Figure 5 Three point bending test setup.

Assuming that the modulus in tension is the same as in compression [68] the following equations, taken from [67] and [68], were used to compute the flexural properties;

1. Maximum Normal Bending Stress (σ_{max})

$$\sigma_{max} = \frac{Mh}{2I} \tag{14}$$

where,

M = bending moment
h = thickness of the beam
I = moment of inertia of cross-section

2. Bending Moment (M)

$$M = \frac{PL}{4} \tag{15}$$

where,

P = load at center of beam
L = beam span

3. Moment of Inertia (I)

$$I = \frac{wh^3}{12} \tag{16}$$

where,

w = beam width

Substituting into eq. (14) gives

$$\sigma_{max} = \frac{3PL}{2wh^2} \tag{17}$$

4. Flexural modulus (E_f)

$$E_f = \frac{PL^3}{4wh^3\left[\delta - \frac{3PL}{8whG_{13}}\right]} \tag{18}$$

where,

δ = deflection at beam center
G_{13} = interlaminar shear modulus

Recognizing that the shear deformation modulus is negligible due to the high span/thickness ratio [67], leads to a simplified version of eq. (18) where P/δ is the slope of the load-deflection curve.

$$E_f = \frac{PL^3}{4wh^3\delta} \tag{19}$$

The strain of the outer fiber at the center of deflection was calculated by using the following equation, obtained from [69];

$$\varepsilon = \frac{6\delta h}{L^2} \tag{20}$$

2.4 Scanning Electron Microscopy

Two test specimens were chosen at random from each test group for scanning electron microscopy analysis. The cross-section of the failure site was gold coated, at 50 millitorr, using a Denton Vacuum Etch/Sputter System (Desk 1 Model). The coated specimens were examined via a Jeol (Model No. JSM-T300) scanning electron microscope. The tensile test specimens were examined at a 45° angle from the horizontal. The flexural specimens were examined by looking at the tension side of the failure (lower outer fiber) and side view of the failure site. Black and white Polaroid photographs were taken at various magnification to help elucidate the failure mechanism.

2.5 Fiber Volume Fraction Analysis

The volume fraction was calculated before fabrication by converting the fiber weight percent to volume percent. To confirm this calculation after fabrication, the cross-sectional area of two specimens out of 10 samples were examined at random. The samples were potted in epoxy and the cross-section was polished using #600 grit sandpaper. The samples were gold coated. The Quantum Kevex Image Analysis System (Delta 2 Model) was used in conjunction with the SEM. This system allows the user to select an area of interest and select certain features by using the color spectrum. The SEM was set for backscatter scanning mode. The white pixels on the screen indicated the CaP fibers, while the dark ones referred to the polymer (Fig. 6). Three areas (69,000-μm^2 each) were chosen at random from each specimen. The magnification was held constant (350X) for all measurements. The imaging system calculated the percent area occupied by the fiber. The mean and standard deviation was calculated for each area measurement. Lower magnification (35X) pictures were also taken for relative comparison of larger areas between the three fiber volume concentrations.

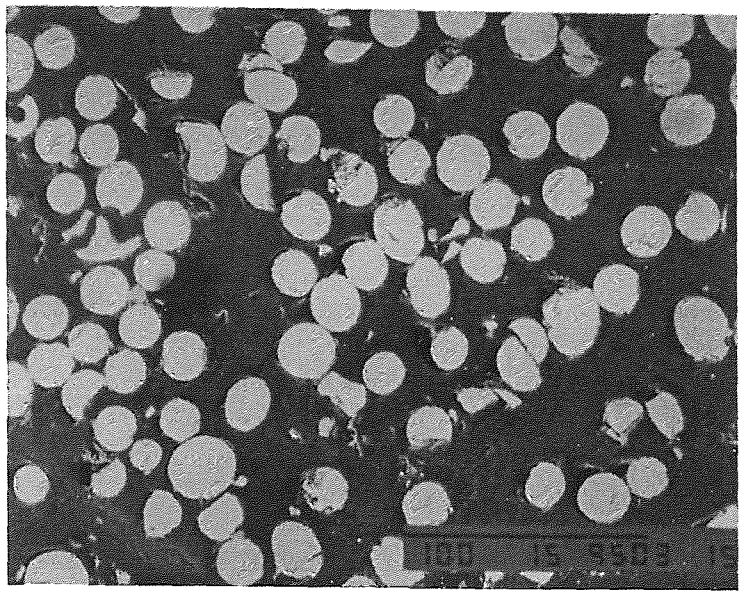

Figure 6 Typical SEM micrograph for volume fraction analysis (40% non-treated fiber at 350X).

2.6 Gel Permeation Chromatography

Gel permeation chromatography was used to determine the degradation of the polymer matrix during processing. A small sample of material (polymer or composite) was chosen at random from the fabricated sheets. The specimens were shipped to Dr. Yuelie Lu (Dept. of Chemistry, Rutgers University, Piscataway, NJ) for analysis. The composite specimens were first dissolved in methylene chloride and then the fibers were filtered out. Once the solvent evaporated this poly(DTE) was used in the GPC analysis.

Molecular weights were obtained by GPC on a system consisting of a Perkin Elmer pump (Model 410) and a Waters differential refractometer (Model 410). Two PL-gel columns (Polymer Laboratories) with pore sizes 10^3 and 10^5 Å were operated in series in THF (1 ml/min). Molecular weights were reported as weight averages relative to polystyrene standards. The "virgin" poly(DTE carbonate) (68,000 da M_w) was used to check the apparatus accuracy.

CHAPTER 3

RESULTS AND DISCUSSION

3.1 Analytical Calculations of the Chopped Fiber Composite

The SMC software package predicted that a fiber aspect ratio (length/diameter) greater than 100 would optimize the modulus of the DTE/CaP discontinuous random-planar fiber composite. Figure 7 depicts the effect that the aspect ratio has on the elastic modulus of the composite. There was no noticeable gain in modulus by going to an aspect ratio greater than 100. Since the CaP fibers have a nominal diameter of 20 μm, a 100 aspect ratio corresponds to a 2 mm long fiber. It was observed, that larger fibers resulted in less dense packing and more voids. A compromise was reached and the fiber length specification was set between 2- and 4-mm.

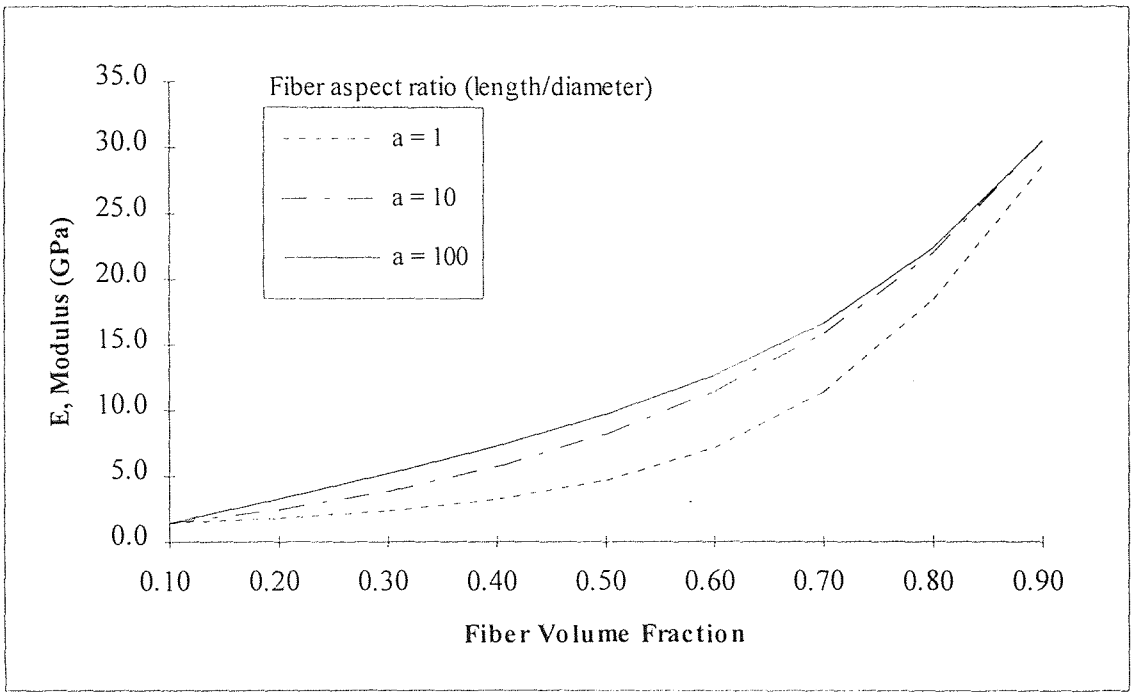

Figure 7 Fiber aspect ratio effect on the elastic modulus of DTE/CaP random-planar chopped fiber composite.

The theoretical values for the elastic modulus of the DTE/CaP composite system are shown in Table 3. It should be pointed out that these results are based on the assumptions discussed in the previous sections. These values should only be used to judge the performance of the manufacturing process, as well as the fiber/matrix coupling efficiency. The theoretical values represent an upper bound which may never be achieved, but one could strive to approach them by optimizing the various parameters which affect the composite performance.

Table 3 SMC theoretical elastic modulus for the DTE/CaP chopped random-planar composite system.

Fiber Vol. %	Elastic Modulus, GPa
20	3.3
30	5.2
40	7.3

3.2 Mechanical Tests of the Neat DTE Polymer

3.2.1 Tensile Test

The tensile test results of the neat DTE polymer are shown in appendix I (Table 4). Some specimens failed near the grip area, indicating a failure due to stress concentrations near the grips. These data points were removed from the mean and standard deviation calculations. The breaking strength fell within previously reported values [38] of 67 MPa ±23 MPa. However, the mode of failure this time was more ductile. Figure 8 illustrates a typical tensile stress-strain plot of the neat DTE. Figures 9a)-b) and 10a)-b) illustrate the failure mechanism through SEM. The tensile modulus of the DTE polycarbonate (1.46 GPa) was lower than that of industrial grade polycarbonates (≈ 2.2 GPa) [70]. This can probably be attributed to the greater backbone flexibility of the DTE polymer versus that of polycarbonate.

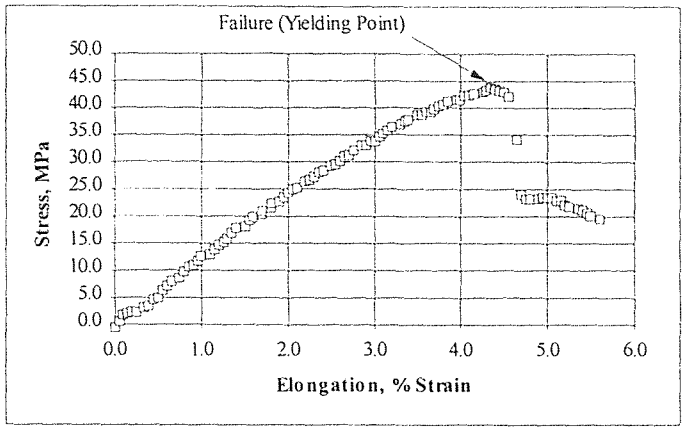

Figure 8 Typical tensile stress-strain curve for the neat DTE polymer (specimen No. 2).

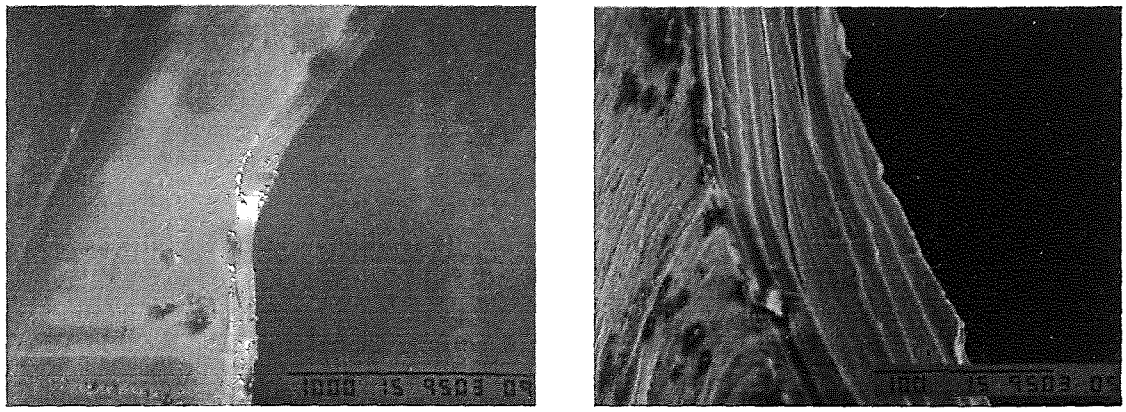

Figures 9a) and **9b)** DTE polymer tensile test failure site (50X and 350X, respectively).

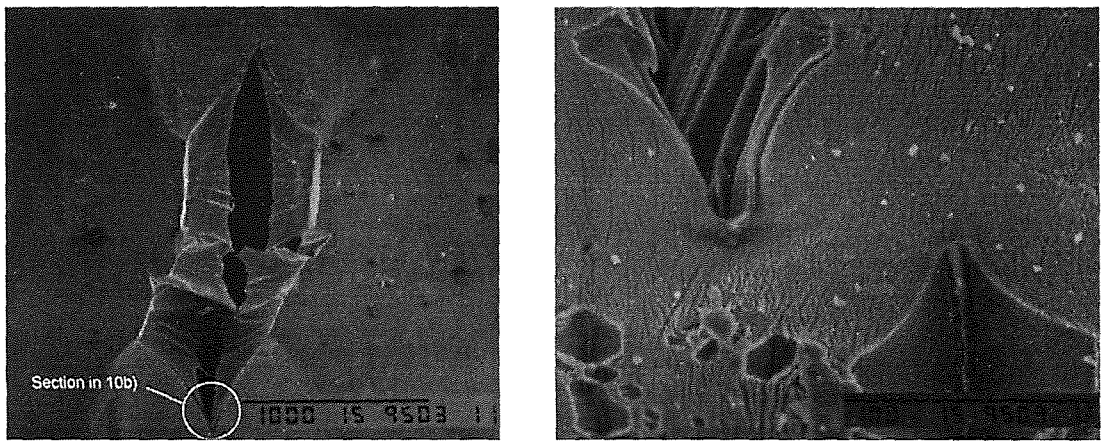

Figures 10a) and **10b)** Typical crack propagation in neat DTE tensile test specimens (35X and 500X respectively).

3.2.2 Flexural Test

The three point bending test for the neat DTE yielded only flexural modulus information for the four specimens tested (Table 5 in appendix I). None of the specimens failed before or at the full deflection (6 mm or ≈ 2.2% strain) employed in this test (Fig. 11). Higher deflections were not used since the specimen would then start to slip and fall through the two outer beam supports. The mean flexural modulus was somewhat lower than the mean tensile modulus of the neat polymer. This may be attributed to error buildup from using very thin testing specimens.

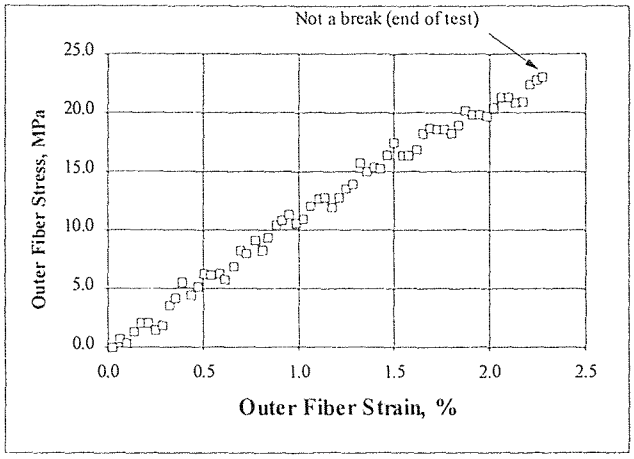

Figure 11 Typical flexural test stress-strain plot for neat DTE (specimen No. 1).

3.3 Mechanical Tests of the Chopped Fiber Composite

3.3.1 Tensile Test

As expected, all of the chopped fiber composite specimens had higher tensile modulus than the neat polymer. Some of the specimens, as with the neat polymer, failed too close to the grip area, and they were not included in the mean and standard deviation calculations. The mechanical results for each specimen are included in appendix I (Tables 6-11). Figures 12a) and 12b) depict the stress-strain curves for typical non-treated and plasma treated composites respectively.

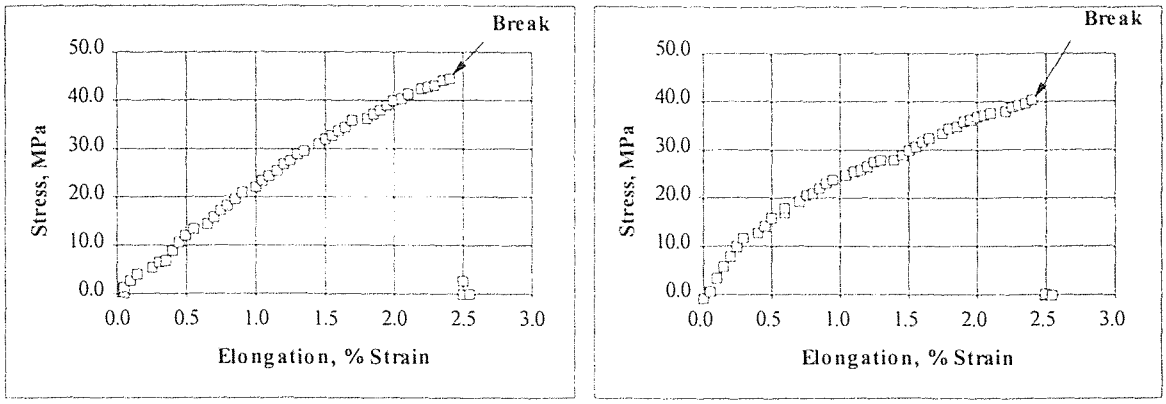

Figures 12a) and **12b)** Typical tensile test stress-strain curves for non-treated and plasma treated 30% fiber composite specimens, respectively (specimens No. 7).

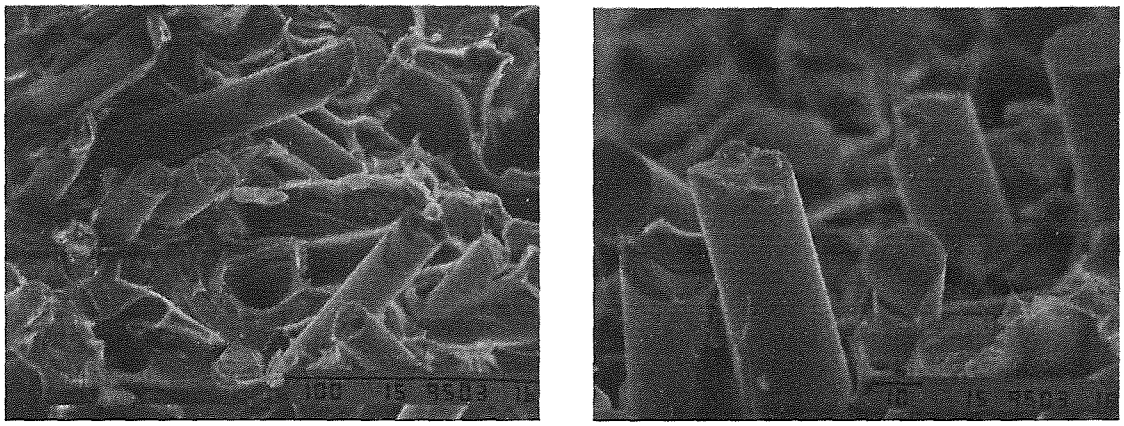

Figures 13a) and **13b)** Non-treated chopped fiber composite failure site by tensile testing (500X and 1000X, respectively). Note the long "clean" fibers and holes.

The untreated fiber composites had greater tensile modulus than the neat polymer by 49-55% and increased with fiber volume fraction. The contribution of going to a higher fiber volume fraction was not statistically significant. This is possibly due to poor fiber-matrix coupling. SEM examination of the untreated composites revealed "clean" fibers and holes in the matrix at the failure site, both of which phenomena are indicative of poor coupling [71]; see Fig(s). 13a) and 13b). The primary mode of failure for the untreated short fiber composites is thought to be first by fiber debonding followed by

fiber pullout and ending in matrix fracture. This failure mode is typically found in composites with poor interfacial bonding [72].

The plasma treated fibers had a tensile modulus 16-40% higher than the non-treated fibers (Fig. 14). An unpaired t-test with unequal variances and a 95% confidence level, showed that at 20%, 30% and 40% there was considerable statistical significance ($p < 0.002$ respectively) between the treated and non-treated tensile moduli. Overall, the treated fibers increased the tensile modulus of the neat polymer by 74-116% as the fiber volume fraction was increased from 20% to 40%.

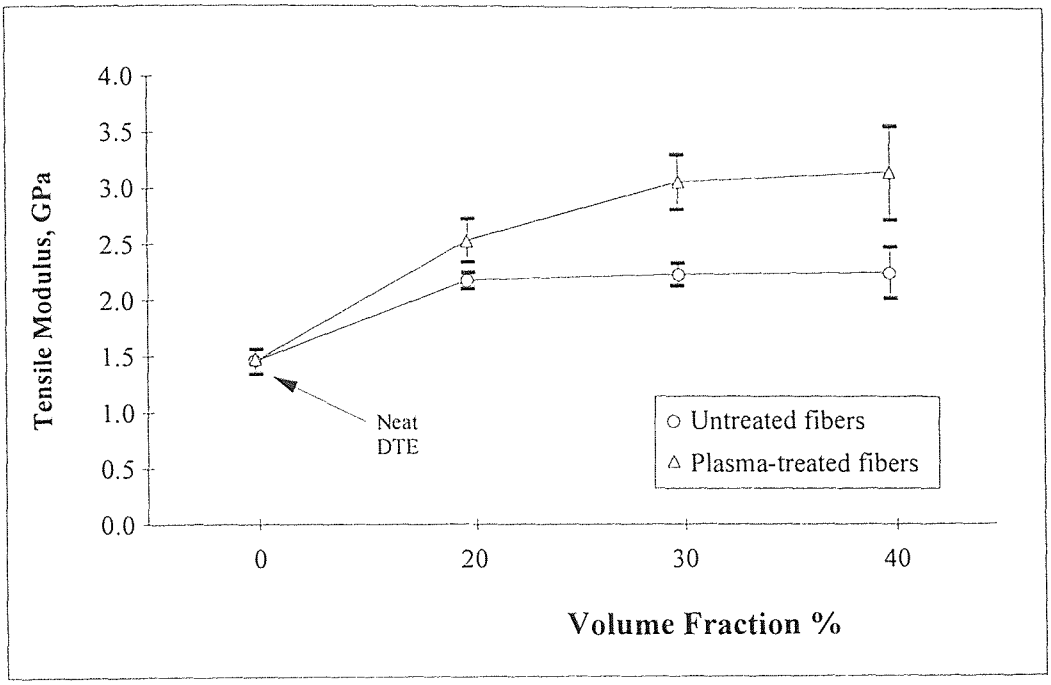

Figure 14 Effect of plasma treatment on the tensile modulus of DTE/CaP random-planar chopped fiber composite.

The SEM analysis showed that the treated fibers at the failure site had some polymer attached to them, Fig(s) 15a) and 15b). Also, the fiber pullout length seemed much shorter than in the untreated composite (Fig. 16, in appendix II). The SEM micrographs represent only a small section of a particular specimen and not the entire

failure site nor all of the specimens. There were also "clean" fibers in the plasma treated composites, but for the majority of the cases the pulled-out fibers had polymer attached to their surface. The mode of failure in this case, is similar to the non-treated fiber composites, but differs in that the fiber pullout strength is higher, allowing the more opportunity for fiber fracture which increases the stiffness. There was no statistical significant difference between the modulus of the 30% and 40% plasma treated fiber composites ($p < 0.6$), may be due to poor fabrication technique: as the fiber volume fraction increased, more voids and defects were introduced into the composite.

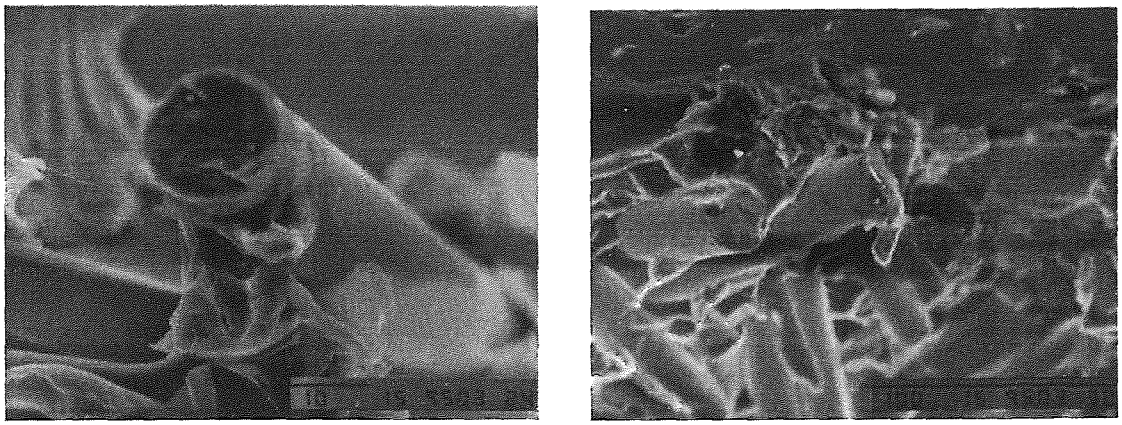

Figures 15a) and **15b)** Plasma-treated chopped fiber composite failure site by tensile testing (1,500X and 500X, respectively).

The nominal breaking strength of both the plasma treated and non-treated chopped fiber composites was slightly lower than the neat polymer (Fig. 17); however, there was no significant statistical difference. The small changes can be accounted for by the fact that the composite does have more voids and defects than the neat polymer which are inherit in the manufacturing process (Fig. 18).

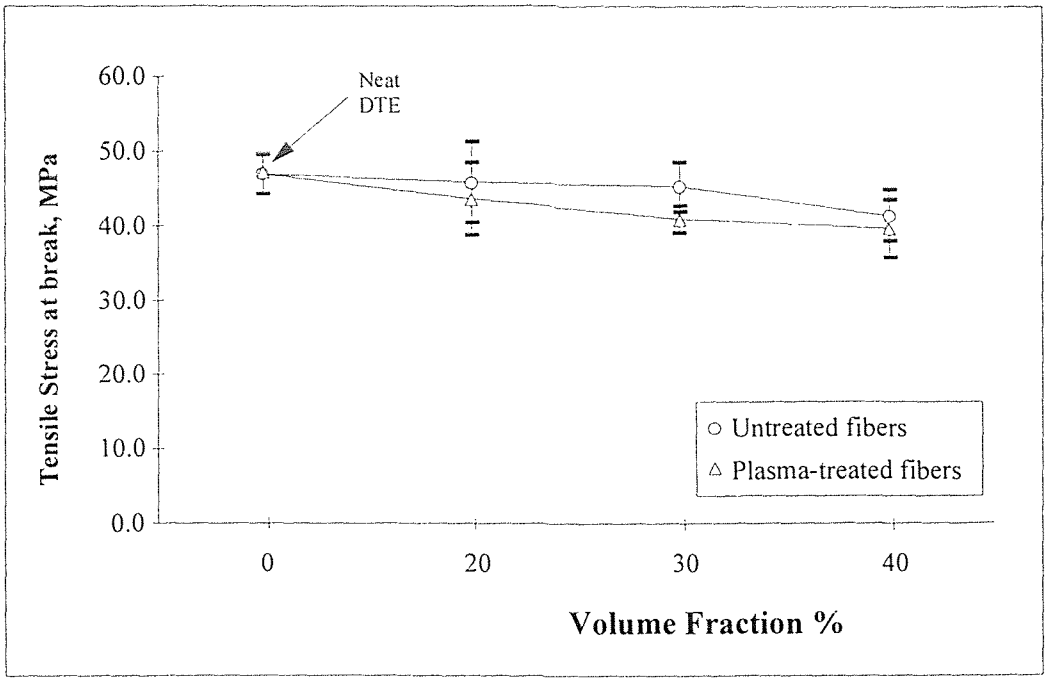

Figure 17 Effect of plasma treatment on the tensile strength of DTE/CaP random-planar chopped fiber composite.

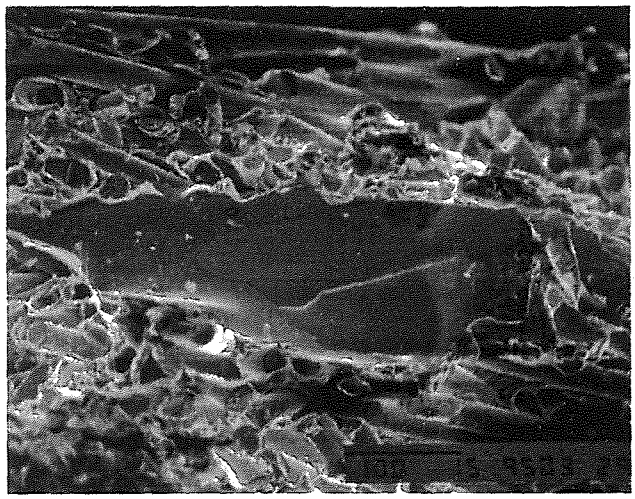

Figure 18 Non-uniform fiber distribution caused by poor manufacturing techniques (200X).

3.3.2 Flexural Test

The three point bending test did not yield any bending strength data for the 20% fiber composites since not enough specimens broke (Tables 12 and 13, in appendix I) to provide statistically significant results. The higher fiber percent specimens broke, for the most part, during the course of the test (Tables 14-17, in appendix I). The flexural strength for both 30% and 40% composites was higher than their tensile strength. According to the literature flexural strength is often higher than tensile strength [69] [73]. This is usually attributed to the statistical nature of the failure process. In the flexure specimen, the maximum stress is attained only at the "outer fiber," while in a tensile specimen it is attained across the sample cross-section [69]. Thus, the probability of finding a critical flaw or defect in the flex specimen is less than in the tensile specimen. The SEM analysis showed that there were large fiber concentrations on the surface of the specimens as seen in Fig(s). 19 (below) and 20 (appendix II).

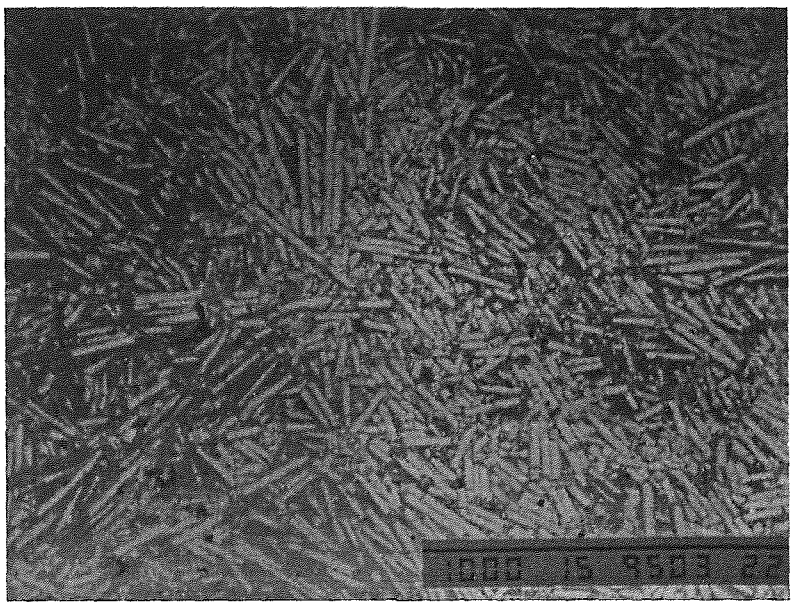

Figure 19 Random chopped fiber concentration on the composite surface (50X).

There was no statistical significant differences between the untreated and plasma-treated composite flexural strengths (Fig. 21). The bending failure mechanism is quite different from the mechanism of tensile failure. In bending the fibers above the neutral axis are in compression, while the ones below experience tension. Figures 22a) and 22b) and Fig. 23 (appendix II) depict the failure site of a flexural specimen. The large space surrounding the fibers (Fig. 24, appendix II) indicates that the fibers experience stresses at an angle, which is common in flexural tests.

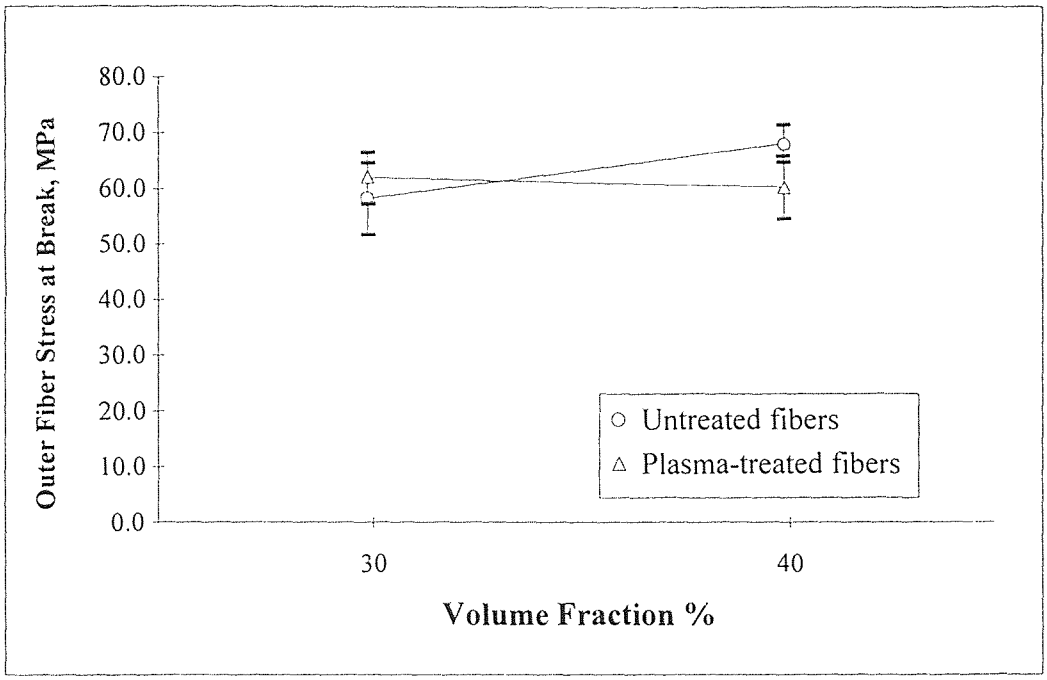

Figure 21 Effect of plasma treatment on the flexural strength of DTE/CaP random-planar chopped fiber composite.

The flexural modulus of all three fiber volume concentrations for both untreated and treated fibers was significantly higher than their tensile moduli. It was thought that this may be explained by the differences in testing speed. The flexural test was performed at a higher cross-head speed than the tensile test (5 mm/min vs. 0.2 mm/min). It has been shown that higher strain rates do in fact yield higher elastic modulus in

polymeric materials due to their viscoelastic behavior, [74] [75]. However, if this were the case, the flexural modulus for the neat DTE would also follow this trend. Since the neat DTE bending modulus was actually lower than the tensile modulus, the strain rate effect does not seem to explain this discrepancy, assuming both flexural and tensile specimens degraded equally during processing.

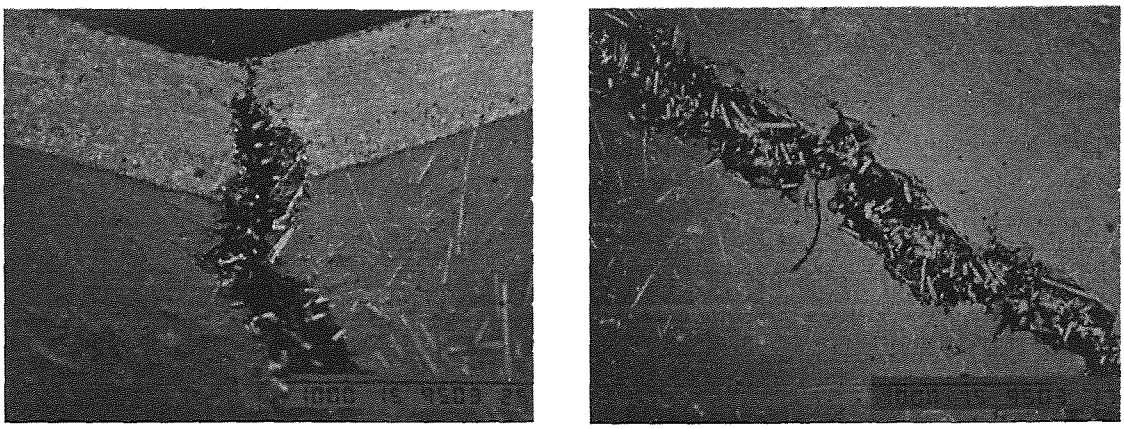

Figure 22a) and **22b)** Tensile side of a 30% chopped fiber composite specimen after flexural failure (50X and 35X, respectively).

Any variation in properties (i.e. fiber amount, voids and defects) between the sample skin and the core will be amplified in the flexural test [69]. Non-isotropic conditions and the previous assumption of equal moduli in compression and tension is inadequate. It seems that the "true" neutral axis of the bending composite specimens tends to shift downward. If the former is true, then the specimens would experience more of a compression effect. The neutral axis shifting hypothesis would probably be more prevailing in the composites with the lower fiber amount, since the variation in fiber distribution would be greater. In fact, the bending modulus of the 20% fiber composites (3.10 GPa) closely approaches the theoretical value of 3.3 GPa.

Another factor which could explain these discrepancies is the fact that the bending test specimens were very thin. The thickness measurements were done at three locations

in each specimen and the mean thickness was used in the modulus and strength calculations. In some instances the standard deviation was as high as ±0.1-mm for a mean specimen thickness of 0.6-mm. After closely examining the beam equations, a very small error in thickness would result in a large error in the stress and modulus computations, since the thickness is raised to the second and third power, respectively. The author suggests that in future studies thicker test specimens should be used in order to validate this data.

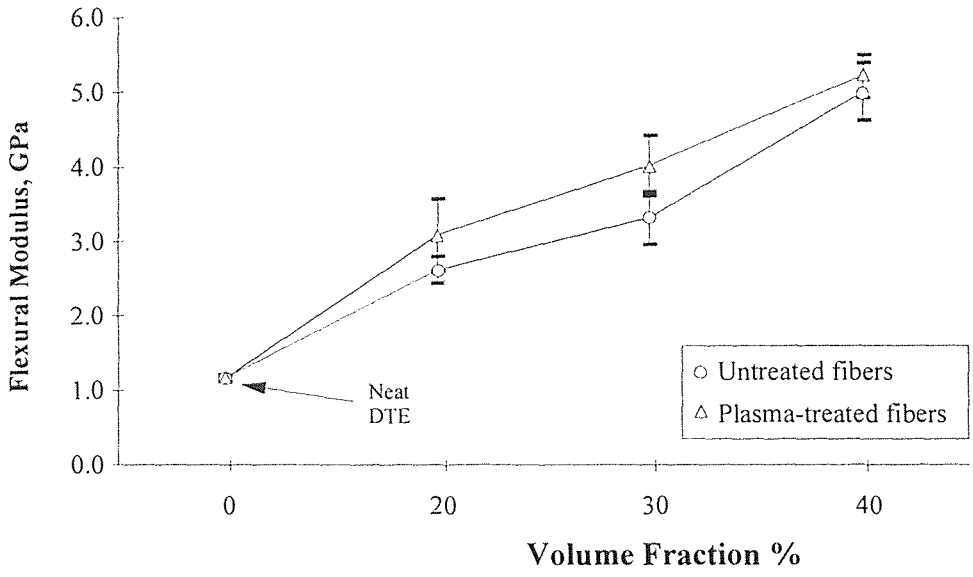

Figure 25 Effect of plasma treatment on the flexural modulus of DTE/CaP random-planar chopped fiber composite.

The effect of the plasma treatment on the bending moduli is depicted in Fig. 25. Only the flexural modulus of the 30% plasma-treated composites was statistically significantly different from the untreated specimens ($p < 0.0004$). Typical flexural stress-strain plots for the 30% untreated and treated composites are illustrated in Fig(s). 26a) and 26b). The SEM examination of the failure site did show clean fibers in the untreated specimens vs. some fibers with polymer attached in the plasma treated specimens, see Fig(s). 27a) and 27b). However, this was not seen as much as with the tensile test

specimens. These results support the drafted hypothesis, since the coupling effect would not play a significant role in the flexural stiffness if compression is in fact the major contributor. In compression the fibers and matrix are pushed against one another, while in tension they are pulled apart leading to debonding.

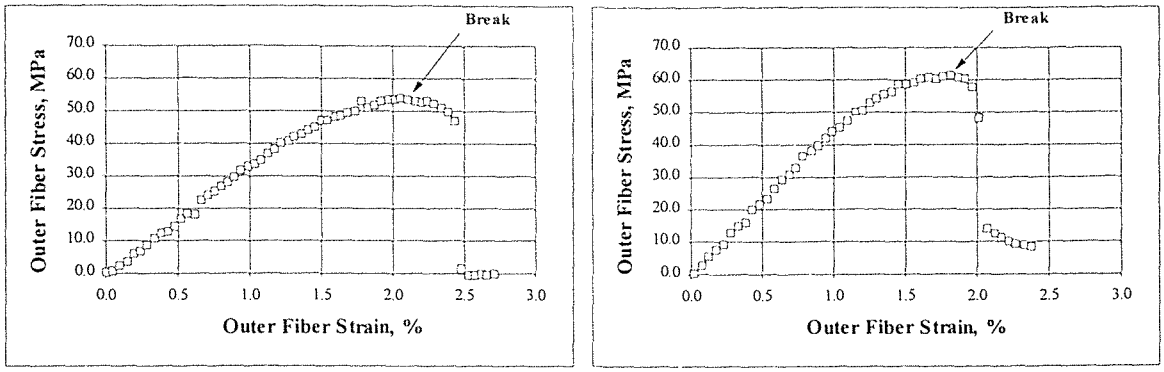

Figures 26a) and **26b)** Typical flexural test stress-strain curves for non-treated and plasma treated 30% fiber composite specimens, respectively (specimens No. 2 & 7).

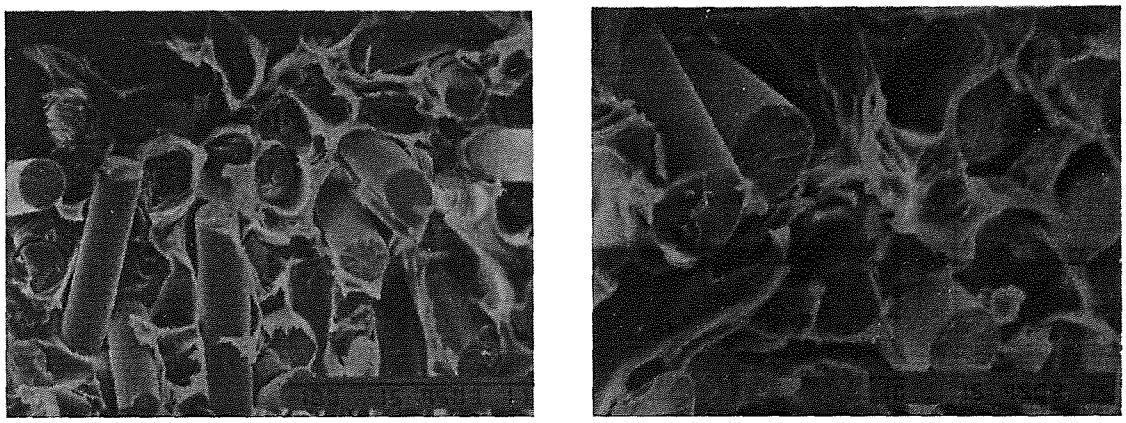

Figure 27a) and **27b)** Failure site of an untreated and plasma-treated bending test specimens (500X and 750X, respectively).

3.4 Volume Fraction Analysis Results

The volume fraction analysis revealed that there are variations in the amount of fiber distribution throughout the composites. For example, Table 18 shows that one of the 20% specimens had only about 11% fiber.

Statistically the photomicrographic technique requires many samples in order to produce reliable results, due to the small area that is viewed [67]. However, these results could also indicate that there are variations which are unavoidable with the fabrication techniques employed in this work. Figure 28, below shows that there were some relative differences in the fiber amount of the chopped fiber composites. Complete results for this analysis can be found in appendix I and II (Tables 19-21 and Figures 29-34, respectively).

Table 18 Volume fraction measurements for the non-treated tensile test specimens.

Location No.	20% theoretical fiber volume		30% theoretical fiber volume		40% theoretical fiber volume	
1	11.00	19.56	36.18	33.32	36.73	36.69
2	10.79	26.72	23.84	23.92	33.97	44.30
3	10.90	12.26	33.70	34.51	35.77	32.62
Mean	10.90	19.51	31.24	30.58	35.49	37.87
STDEV	0.110	7.23	6.53	5.80	1.40	5.93

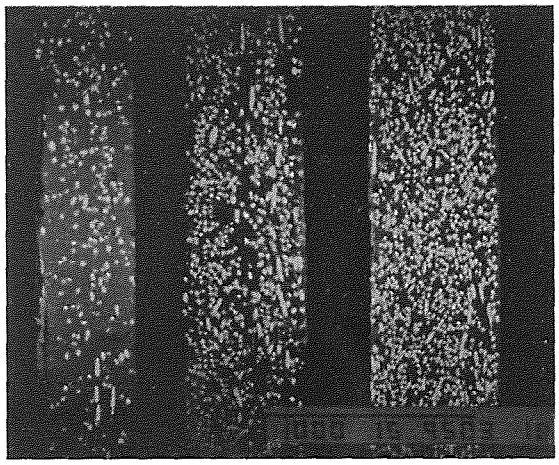

Figure 28 Cross-section showing fiber amount (20%, 30% and 40% left to right) in three untreated tensile test specimens (35X).

3.5 Gel Permeation Chromatography Analysis Results

The GPC analysis (Table 22) showed that there was some degradation (≈ 14%) during processing for the neat DTE polymer. The non-treated composites lost about 18% of their initial molecular weight, while the plasma-treated composites lost about 17%. There was no statistical significant differences in processing degradation between the neat DTE and the non-treated or the neat DTE and the plasma-treated composites ($p < 0.025$). In addition, there weren't any statistical significant differences between the degradation of the non-treated and plasma-treated composites ($p < 0.59$) due to processing. The statistical significance was computed using an unpaired t-test, assuming unequal variances, with a 95% confidence level. A more complete history of the processing parameters and molecular weight is listed in the appendix (Table 23).

Table 22 GPC analysis results for the tensile test specimens.

"Virgin" DTE (before process)	M_W after processing		
	Neat DTE	Non-Treated	Plasma-treated
69,000	60,050	57,705	56,426
—	59,266	54,128	56,120
—	—	55,881	56,575
—	—	55,675	58,765
—	—	59,865	57,537
—	—	57,520	58,533
Mean	59,658	56,796	57,326
STDEV	554.4	1,999	1,131

CHAPTER 4

CONCLUSIONS & RECOMMENDATIONS

4.1 Conclusions

The mechanical properties of a totally bioabsorbable composite material were obtained via tensile and flexural testing. The matrix material used was a poly-(desamino-tyrosyl-tyrosine ethyl ester)-carbonate (DTE) and it was reinforced with an absorbable calcium phosphate (CaP) glass fiber. A methane plasma treatment was used to improve the fiber-matrix coupling.

All fabrication was done via compression molding. The chopped fiber composites were fabricated using a prepreg method. Teflon sheeting proved to be an effective way to prevent the materials from sticking to the mold surfaces. The processing temperature of 116 °C was adequate to fill the entire mold cavity and minimize polymer degradation. The GPC analysis demonstrated that a maximum of 18% molecular weight loss was encountered by using these processing parameters. The volume fraction analysis indicated significant fiber volume concentration gradients which were unavoidable with the fabrication techniques employed in this work.

The tensile tests results for the neat polymer were consistent with published data. However, the mode of failure this time was more ductile. The tensile modulus of neat DTE (1.46 GPa) along with other biocompatability features, makes this absorbable polymer a good candidate to compete with other materials such as poly-p-dioxanone, poly-ε-caprolactone and poly-o-ester in the fracture fixation arena. The neat DTE flexural modulus was lower (1.16 GPa) than the tensile modulus. It is suspected that using very thin testing specimens caused this discrepancy via error buildup. None of the neat polymer specimens failed during the bending test.

The SMC computer program (University of Delaware Center for Composite Materials), was used to predict the elastic properties of the DTE/CaP discontinuous fiber composites. The program suggested that an optimum elastic modulus would be obtained if the fiber aspect ratio (length/diameter) was kept greater than 100, which corresponds to a fiber length greater than 2-mm for 20-μm diameter fibers. Theoretical predictions of the moduli were 3.3, 5.2 and 7.3 GPa for 20, 30 and 40% fiber by volume, respectively.

Plasma treatment of the CaP fibers provided a moderate improvement in the modulus of the chopped fiber composites. The tensile strength was not improved by this coupling method. The treated fiber composites had a tensile modulus 16-40% higher than that of untreated fiber composites. In addition, treating the fibers increased the tensile modulus of the neat polymer by more than 115%. The tensile modulus was not improved significantly by further increasing the fiber volume above 30%. SEM micrographs revealed shorter fiber pullout length and polymer attached to fiber ends in the treated fiber composites while in the untreated fiber composites, more holes and longer "clean" fibers were observed.

It is believed that the tensile and compression modulus of this composite material are not equal. The flexural test results support this hypothesis. The breaking strength in bending was higher than in tensile loading; a common phenomenon with materials that are weaker in tension than in compression. The neutral axis of such a material would shift towards the tensile side of the specimen being tested. The flexural modulus was higher than the tensile modulus and in some cases it approached the theoretical value. There were no statistically significant differences in flexural modulus between the treated and untreated fiber composites, except at the 30% fiber volume. In compression the coupling does not have an effect on the mechanical properties, since the fibers and matrix are pushed against one another, while in tension the coupling delays the debonding of the fiber from the matrix.

In their present form, these composite materials are not suitable for high load applications; for the fixation of long bones such as femurs. Recent reports have described the clinical use of biodegradable rods and screws for the fixation of bimalleolar fractures of the ankle, intra-articular fractures of the elbow joint, and for bony avulsions [3]. CaP-reinforced DTE may be suitable for these applications provided it retains strength and stiffness long enough to support proper healing.

4.2 Recommendations for Future Work

Although the results of this work are encouraging there is room for improvement. Better fabrication techniques should be employed in the future to further improve the mechanical properties of these materials. For example, polymer degradation can be reduced by molding in an inert atmosphere. Also, the molding pressure should be lowered to reduce the manufacturing cost associated with high pressure molding equipment.

With regards to the mechanical tests, ASTM standard sized specimens should be employed in future tests as more materials and larger molds become available. The flexural test specimens should be thicker in size, but a large span/thickness ratio should be maintained. The strain rate effect on the polymer and composite test specimens should be investigated in more detail. GPC should be performed on both tensile and bending test specimens. New flexural equations should be derived from the beam theory to account for the anisotropy of a discontinuous fiber composite. These suggestions may help elucidate the neutral axis shifting hypothesis presented in this work. Finally, the mechanical properties of other forms of tyrosine-derived polycarbonates, such as DTH and copolymers of such, should be studied in this same manner.

APPENDIX I

EXPERIMENTAL RESULTS DATA

Table 4 Tensile test results for the neat DTE specimens.

Specimen No.	Yielding Stress MPa	Elongation % Strain	Tensile Modulus GPa
1	50.5	4.8	1.51
2	43.9	4.4	1.26
3*	49.5	5.5	1.11
4	46.3	4.1	1.49
5	47.2	4.2	1.47
6*	51.1	5.0	1.56
7	44.7	4.2	1.60
8*	42.7	4.0	1.44
9*	50.6	6.0	1.35
10	49.6	5.6	1.41
Mean	47.0	4.5	1.46
STDEV	2.61	0.581	0.112

* Failure near grips (data point thrown out from all mean/stdev calculations)

Table 5 Flexural test results for the neat DTE specimens.

Specimen No.	Flexural Modulus GPa
1	1.18
2	1.20
3	1.19
4	1.10
Mean	1.16
STDEV	0.466

Note: None of the specimens broke, but all had stress crazing and permanent deformation.

Table 6 Tensile test results for the 20% non-treated chopped fiber composite specimens.

Specimen No.	Stress at break MPa	Elongation at break % Strain	Tensile Modulus GPa
1*	22.5	1.1	2.48
2*	38.7	2.3	1.98
3	40.1	2.1	2.20
4	40.0	2.2	2.17
5*	40.7	2.2	2.18
6	49.8	3.2	2.15
7	49.4	2.7	2.26
8	43.6	2.6	2.06
9	52.6	2.9	2.18
10*	55.7	3.6	1.82
Mean	45.9	2.6	2.18
STDEV	5.39	0.418	0.076

* Failure near grips (data point thrown out from all mean/stdev calculations)

Table 7 Tensile test results for the 20% plasma-treated chopped fiber composite specimens.

Specimen No.	Stress at break MPa	Elongation at break % Strain	Tensile Modulus GPa
1*	55.9	3.1	2.62
2	44.8	2.4	2.44
3	47.2	2.6	2.28
4	41.2	2.3	2.57
5	40.8	2.3	2.44
6	48.6	2.1	2.85
7	49.0	2.6	2.81
8	46.7	2.1	2.60
9	40.8	2.1	2.32
10	34.2	1.6	2.56
Mean	43.7	2.2	2.54
STDEV	4.84	0.300	0.197

* Failure near grips (data point thrown out from all mean/stdev calculations)

Table 8 Tensile test results for the 30% non-treated chopped fiber composite specimens.

Specimen No.	Stress at break MPa	Elongation at break % Strain	Tensile Modulus GPa
1	44.6	2.9	2.10
2	40.9	2.4	2.32
3*	43.4	2.7	2.10
4	43.7	2.8	2.15
5*	42.0	3.2	1.95
6	50.4	2.9	2.27
7	44.5	2.4	2.27
8*	49.3	3.5	2.12
9*	41.8	2.3	2.15
10	48.0	2.9	2.37
Mean	45.3	2.7	2.24
STDEV	3.36	0.239	0.103

* Failure near grips (data point thrown out from all mean/stdev calculations)

Table 9 Tensile test results for the 30% plasma-treated chopped fiber composite specimens.

Specimen No.	Stress at break MPa	Elongation at break % Strain	Tensile Modulus GPa
1	43.7	2.5	2.97
2	38.3	1.9	2.86
3*	40.8	2.1	2.60
4	40.7	1.9	2.91
5*	35.2	1.5	3.20
6	41.1	2.0	2.87
7	40.2	2.4	3.17
8	42.4	2.1	3.21
9*	38.3	1.9	2.75
10	39.8	1.9	3.52
Mean	40.9	2.1	3.07
STDEV	1.75	0.263	0.242

* Failure near grips (data point thrown out from all mean/stdev calculations)

Table 10 Tensile test results for the 40% non-treated chopped fiber composite specimens.

Specimen No.	Stress at break MPa	Elongation at break % Strain	Tensile Modulus GPa
1*	35.9	1.8	2.59
2	41.6	2.3	2.20
3	41.1	2.3	2.27
4	41.2	2.1	2.32
5	34.6	1.7	2.04
6	43.9	2.5	2.17
7	39.2	2.1	2.24
8	41.6	2.7	1.93
9	41.7	2.6	2.41
10	47.8	4.1	2.74
Mean	41.4	2.5	2.26
STDEV	3.51	0.665	0.230

* Failure near grips (data point thrown out from all mean/stdev calculations)

Table 11 Tensile test results for the 40% plasma-treated chopped fiber composite specimens.

Specimen No.	Stress at break MPa	Elongation at break % Strain	Tensile Modulus GPa
1*	36.5	1.6	3.16
2	40.1	1.8	3.28
3*	39.0	1.8	2.96
4*	24.9	1.1	2.78
5	35.4	1.5	3.63
6	36.0	1.6	3.09
7	46.0	2.6	2.81
8	39.0	2.1	2.59
9*	34.3	1.7	3.22
10	41.6	2.0	3.58
Mean	39.7	1.9	3.16
STDEV	3.90	0.382	0.416

* Failure near grips (data point thrown out from all mean/stdev calculations)

Table 12 Flexural test results for the 20% non-treated chopped fiber composite specimens.

Specimen No.	Flexural Modulus GPa
1	2.63
2	2.38
3	2.65
4	2.74
5	2.92
6	2.40
7	2.64
8	2.65
9	2.80
10	2.51
Mean	2.63
STDEV	0.170

Note: None of the specimens broke, but all had stress crazing and permanent deformation.

Table 13 Flexural test results for the 20% plasma-treated chopped fiber composite specimens.

Specimen No.	Stress at break MPa	% Strain at break	Flexural Modulus GPa
1*	—	—	2.62
2*	—	—	2.35
3*	—	—	3.22
4**	55.3	2.2	3.41
5**	60.1	2.0	3.76
6*	—	—	2.58
7*	—	—	3.07
8*	—	—	3.14
9**	57.9	1.9	3.85
10*	—	—	3.03
Mean	—	—	3.10
STDEV	—	—	0.492

* Stress crazing and permanent deformation, (no break, data point thrown out for breaking/strain calculations)

** Partial break

Table 14 Flexural test results for the 30% non-treated chopped fiber composite specimens.

Specimen No.	Stress at break MPa	% Strain at break	Flexural Modulus GPa
1***	48.6	2.1	3.02
2**	53.7	2.1	3.37
3***	60.2	2.2	3.50
4*	—	—	2.91
5***	48.3	2.6	2.77
6***	62.6	2.7	3.18
7**	65.8	2.6	3.44
8***	62.0	2.2	3.72
9***	64.6	2.0	3.95
10***	59.0	2.7	3.10
Mean	58.3	2.4	3.34
STDEV	6.58	0.293	0.363

* Stress crazing and permanent deformation, (no break, data point thrown out for breaking/strain calculations)

** Partial break

*** Complete break

Table 15 Flexural test results for the 30% plasma-treated chopped fiber composite specimens.

Specimen No.	Stress at break MPa	% Strain at break	Flexural Modulus GPa
1	61.2	2.2	3.43
2	74.1	2.0	4.56
3	63.3	2.0	3.91
4	60.3	2.2	3.87
5	63.2	1.9	4.55
6	58.9	1.6	4.14
7	61.3	1.8	4.52
8	59.4	1.8	3.98
9	56.8	1.8	3.66
10	61.1	2.1	3.78
Mean	62.0	1.9	4.04
STDEV	4.71	0.196	0.395

Note: All specimens suffered partial breaks

Table 16 Flexural test results for the 40% non-treated chopped fiber composite specimens.

Specimen No.	Stress at break MPa	% Strain at break	Flexural Modulus GPa
1*	69.4	1.5	5.75
2**	70.3	1.8	5.41
3*	70.4	1.7	5.22
4**	64.2	1.8	4.49
5*	65.3	1.7	4.84
6*	63.9	1.6	4.84
7*	67.4	1.5	5.21
8*	64.7	1.5	4.92
9**	72.7	2.2	4.56
10*	73.5	1.9	4.95
Mean	68.2	1.7	5.02
STDEV	3.56	0.221	0.385

* Partial break

** Complete break

Table 17 Flexural test results for the 40% plasma-treated chopped fiber composite specimens.

Specimen No.	Stress at break MPa	% Strain at break	Flexural Modulus GPa
1	55.2	1.3	4.77
2	56.4	1.1	5.36
3	68.7	1.5	5.81
4	63.5	1.4	5.24
5	63.8	1.5	5.38
6	63.5	1.6	4.98
7	53.5	1.2	5.15
8	52.9	1.2	5.02
9	65.2	1.6	5.22
10	61.4	1.4	5.46
Mean	60.4	1.4	5.24
STDEV	5.47	0.154	0.289

Note: All specimens suffered partial breaks

Table 19 Volume fraction measurements for the plasma-treated tensile test specimens.

Location No.	20% theoretical fiber volume		30% theoretical fiber volume		40% theoretical fiber volume	
1	26.96	18.48	21.48	29.46	38.97	32.75
2	21.57	15.57	25.74	26.91	29.95	43.90
3	15.57	18.81	24.93	27.00	28.49	43.47
Mean	21.37	17.62	24.05	27.79	32.47	40.04
STDEV	5.70	1.78	2.26	1.44	5.68	6.32

Table 20 Volume fraction measurements for the non-treated flexural test specimens.

Location No.	20% theoretical fiber volume		30% theoretical fiber volume		40% theoretical fiber volume	
1	14.14	23.16	22.48	27.65	41.77	42.33
2	14.51	19.30	33.06	26.24	28.46	28.56
3	14.63	15.76	20.51	34.71	29.61	30.69
Mean	14.43	19.41	25.35	29.53	33.28	33.86
STDEV	0.260	3.70	6.75	4.54	7.38	7.41

Table 21 Volume fraction measurements for the plasma-treated flexural test specimens.

Location No.	20% theoretical fiber volume		30% theoretical fiber volume		40% theoretical fiber volume	
1	21.34	25.69	32.96	28.92	30.02	44.37
2	27.38	30.89	36.17	33.09	31.11	45.41
3	16.11	19.62	39.95	23.79	36.46	26.98
Mean	21.61	25.40	36.36	28.60	32.53	38.92
STDEV	5.64	5.64	3.50	4.66	3.45	10.35

Table 23 GPC analysis results and processing data for the tensile test specimens.

Description	Fiber Vol. %	Specimen No.	Processing Press Temp. °C	Processing Peak Temp. °C	M_w	M_n
"Virgin" DTE	—	—	—	—	69,000	29,884
Neat DTE	—	1-5	113	117	60,050	25,654
Neat DTE	—	6-10	99	114	59,266	25,274
Untreated	20	1-5	116	127	57,705	26,609
	20	6-10	117	123	54,128	22,322
fiber	30	1-5	116	125	55,881	24,270
	30	6-10	116	124	55,675	22,595
composites	40	1-5	116	124	59,865	26,916
	40	6-10	116	127	57,520	25,967
Treated	20	1-5	116	125	56,426	24,352
	20	6-10	116	126	56,120	22,329
fiber	30	1-5	116	126	56,575	25,962
	30	6-10	116	127	58,765	25,179
composites	40	1-5	116	123	57,537	28,739
	40	6-10	116	124	58,533	25,319

APPENDIX II

SEM MICROGRAPHS

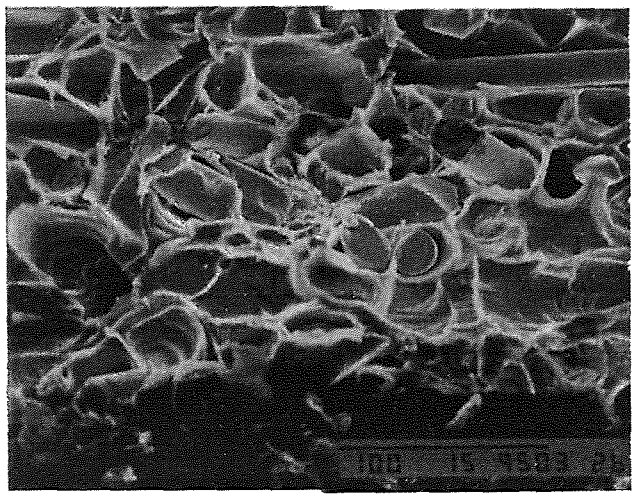

Figure 16 Shorter fiber pullout length in a plasma-treated composite failure site after tensile testing (500X).

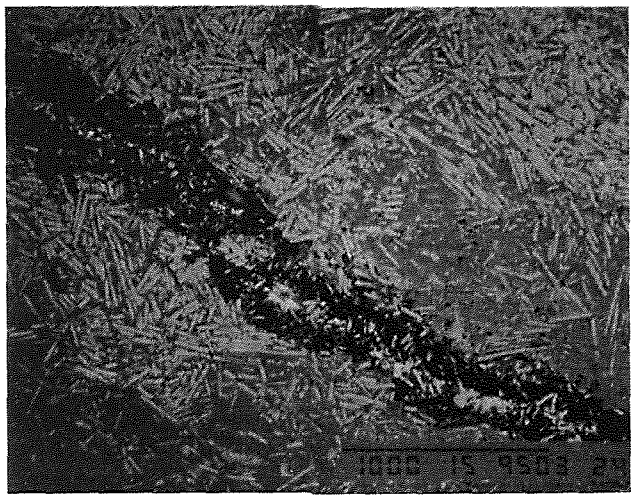

Figure 20 Random chopped fiber concentration on the tensile side surface of a 40% flexural test failed specimen (35X).

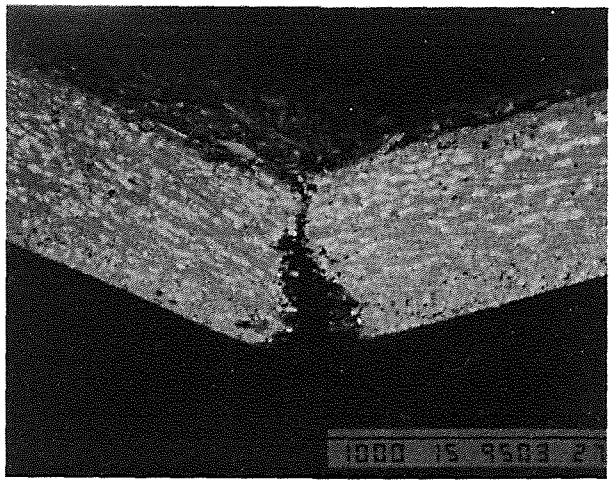

Figure 23 Compression side of a 30% chopped fiber composite specimen after flexural failure (50X).

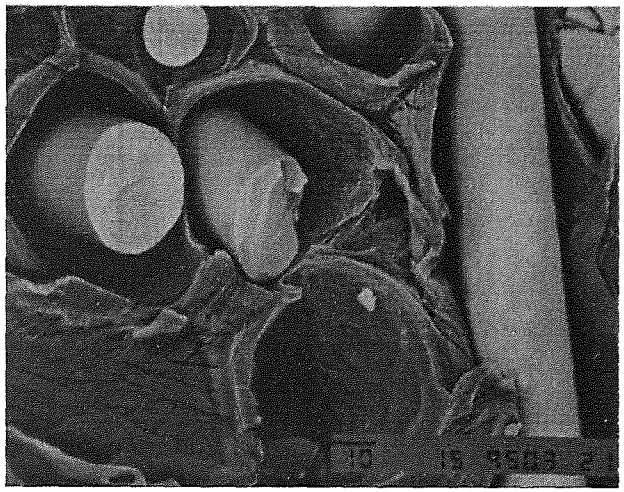

Figure 24 Flexural failure site of a 20% plasma treated fiber composite (750X).

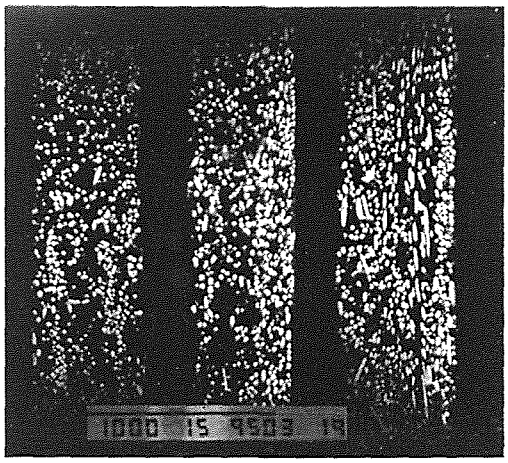

Figure 29 Cross-section showing fiber amount (20%, 30% and 40% left to right) in three plasma-treated tensile test specimens (35X).

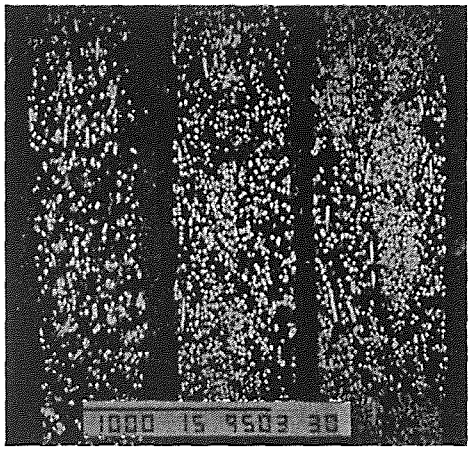

Figure 30 Cross-section showing fiber amount (20%, 30% and 40% left to right) in three untreated flexural test specimens (35X).

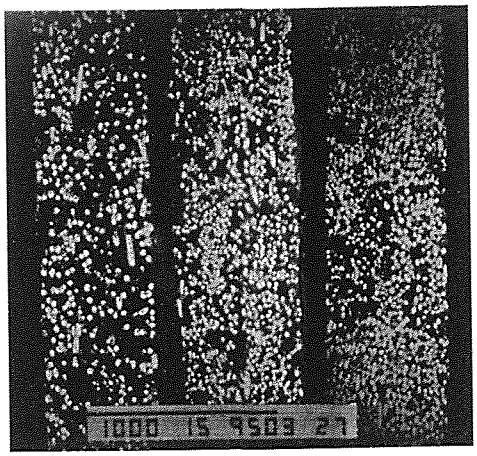

Figure 31 Cross-section showing fiber amount (20%, 30% and 40% left to right) in three plasma-treated flexural test specimens (35X).

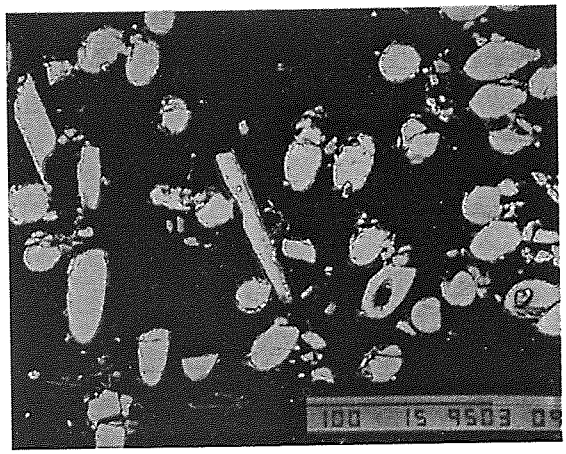

Figure 32 Typical SEM micrograph for volume fraction analysis (20% fiber at 350X).

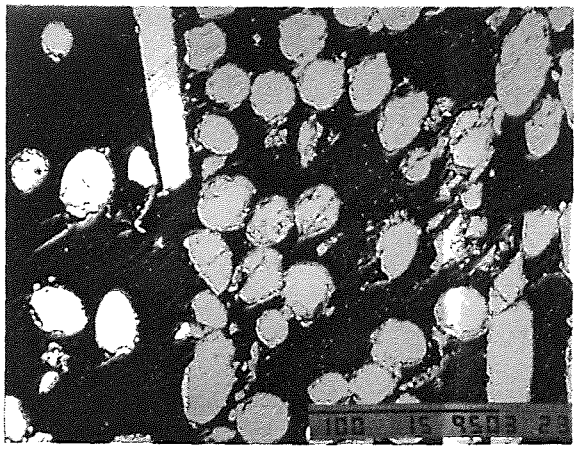

Figure 33 Typical SEM micrograph for volume fraction analysis (30% fiber at 350X).

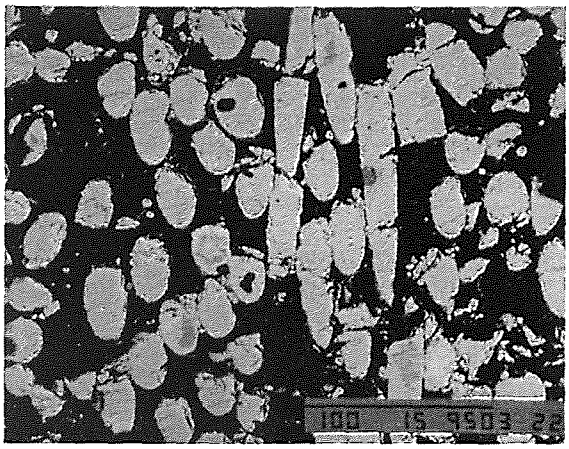

Figure 34 Typical SEM micrograph for volume fraction analysis (40% fiber at 350X).

REFERENCES

1. Zimmerman, M. C. "The design and analysis of absorbable and semi-absorbable composite fracture fixation devices." *Ph.D. Dissertation Rutgers University* (1985).

2. Vander, A. J., J. H. Sherman and D. S. Luciano. *Human Physiology.* 6th ed. New York: McGraw-Hill, Inc., 1994.

3. Tencer, A. F. and Johnson, K. D. *Biomechanics in Orthopedic Trauma.* Philadelphia: J. B. Lippincott Company, 1994.

4. Starr, C. *Biology Concepts and Applications.* California: Wadsworth Publishing Company, 1991.

5. Mears, D. C. *Materials and Orthopaedic Surgery.* Baltimore: The Williams and Wilkins Co., 1979.

6. Curess R. L. and J. Dumont. "Fracture healing." *Can J Surg.* 18 (1975): 403-413.

7. Perren, S. M. "Physical and biological aspects of fracture healing with special reference to internal fixation." *Clin Orthop.* 138 (1975): 175-194.

8. Markel, M. D., M. A. Wikenheiser and E. Y. S. Chao. "A study of fracture callus material properties: relationships to the torsional strength of bone, *J Orthop Res.* 8 (1990): 843-850.

9. Chidgey, L., D. Chakkalakal, A. Blotchky and J. F. Connolly. "Vascular reorganization and return of rigidity in fracture healing." *J Orthop Res.* 8 (1990): 843-850.

10. Hannsmann, H. "Eine neue methode der fixirurig der fregmente bei complicirten fractruen." *Vernhandl Deutsches Gesellsch. f. Chir.* 15 (1886): 134.

11. Danis, R. *Théorie et pratique de l'ostéosynthèse.* Paris: Masson and Cie, 1949.

12. Eggers, G. W. N., T. O. Shindler and C. M. Pomerat. "The influence of the contact-compression factor on osteogenesis in surgical fractures." *J. Bone Jt. Surg.* 31-A (1949): 693.

13. Bagby, G. W. and J. M. Janes. "The effect of compression on the rate of fracture healing using a special plate." *Am. J. Surg.* 95 (1958): 761.

14. Bagby, G. W. "Clinical experience of a simplified compression bone plate." *Am. J. Orthop. Surg.* 10 (1968): 302.

15. —. "Fractures treated with the Bagby compression plate." *J. Bone Jt. Surg.* 57-A (1975): 1031.

16. —. "Compression bone-plating." *J. Bone Jt. Surg.* 59-A (1977): 625.

17. Lindahl, O. "The rigidity of fracture immobilization with plates." *Acta. Orthop. Scand.* 38 (1967): 101.

18. Lawrence, M., M. A. R. Freeman and S.A.V. Swanson. "Engineering considerations in the internal fixation of fractures of the tibial shaft." *J. Bone Jt. Surg.* 51-B (1969): 754.

19. Tayton, K. and J. Bradley. "How stiff should semi-rigid fixation of the human tibia be?" *J. Bone. Jt. Surg.* 65-B (1980): 312.

20. Terjeson, T. and K. Apalset. "The influence of different degrees of stiffness of fixation plates on experimental bone healing." *J. Orthop Res.* 6 (1988): 293-299.

21. Tonino, A. J., C. L. Davidson, P. J. Klopper and L. A. Linclau. "Protection from stress in bone and its effects." *J. Bone. Jt. Surg.* 58-B (1976): 107.

22. Bradley, G. W., G. B. McKenna, H. K. Dunn. A. U. Daniels, and W. O. Statton. "Effects of flexural rigidity of plates on bone healing." *J. Bone Jt. Surg.* 61-A (1979): 866.

23. Langrana, N. A., L. Chow, J. R. Parsons. H. Alexander and A. B. Weiss. "Experimental and analytical investigations of stress protection atrophy with bone plates of varying rigidity." *Advances in Bioengineering* 13 (1982).

24. Sinibaldik, K., H. Rosen, S-K. Lin and M. De Angelis. "Tumors associated with metallic implants in animals." *Clin. Orthop. Rel.* 118 (1976): 257-266.

25. Sunderman, F. W. "Metal carcinogenesis in animals and man." *Food Cosmet. Toxicol.* 9 (1978): 1.

26. McKenna, G. B. "The development of fiber reinforced polymer composites for orthopaedic application." *Ph.D. Dissertation University of Utah* (1976).

27. Parsons, J. R., H. Alexander, S. J. Corcoran and A. B. Weiss. "In vivo evaluation of fiber reinforced absorbable polymer bone plates." *Proceedings of the Second International Symposium on Internal Fixation of Fractures.* Lyon, France (September '82): 355-363.

28. Pulapura S. and J. Kohn. "Trends in the development of bioresorbable polymers for medical applications." *J. of Biomaterials Applications* 6 (1992): 216-250.

29. Böstman, O. M. "Current concepts review. Absorbable implants for the fixation of fractures." *J. Bone Jt. Surg.* 73A (1991): 148-153.

30. Vasenius, J., S. Vainionpää, K. Vihtonen, A. Mäkelä, P. Rokkanen, M. Mero and P. Törmälä. "Comparison of in vitro hydrolysis, subcutaneous and intrmedullary implantation to evaluate the strength retention of absorbable osteosynthesis implants." *Biomaterials* 11 (1990): 501-504.

31. Kulkarni R. K., E. G. Moore, A. F. Hegyeli and F. Leonard. "Biodegradable poly(lactic acid) polymers." *J. Biomed. Mater. Res.* 5 (1971): 169-181.

32. Getter, L., D. E. Cutright, S. N. Bhaskar and J. K. Augsburg. "A biodegradable interosseous appliance in the treatment of mandibular fractures." *J. Oral. Surg.* 30 (1972): 344-348.

33. Böstman, O. M., E. Hirvensalo, J. Mäkinen andP. Rokkanen. "Foreign-body reactions to fracture fixation implants of biodegradable synthetic polymers." *J. Bone Jt. Surg.* 72B (1990): 592-596.

34. Suganuma, J., H. Alexander and J. L. Ricci. "Biological response of intramedullary bone to poly-L-lactic acid." *Mater Res. Soc. Simp. Proc.* 252 (1992) 131-146.

35. Daniels A. U., M. S. Taylor, K. P. Andriano and J. Heller. "Toxicity of absorbable polymers proposed for fracture fixation devices." *Trans 38th Ann. Mtg. Orthop. Res. Soc.* 17 (1992): 88.

36. Zhou, J., S. I. Ertel, H. M. Buettner and J. Kohn. "Evaluation of tyrosine-derived pseudo-poly(amino acids): In vitro cell interactions." *The 20th Annual Meeting of the Society of Biomaterials* (1994): 371.

37. Ertel, S. I., R. Parsons and J. Kohn. "Investigation of a tyrosine-derived polycarbonate as a potential orthopaedic implant." *Trans 19th Ann Mtg Soc Biomater.* (1993): 17.

38. Ertel, S. I. and J. Kohn. "Evaluation of a series of tyrosine-derived polycarbonates as degradable biomaterials." *J. Biomed. Mater. Res.* 28 (1994): 1-12.

39. Daniels, A. U., M. K. O. Chang, K. P. Andriano and J. Heller. "Mechanical properties of biodegradable polymers and composites proposed for internal fixation of bone." *J. Appl. Biomaterials* 1 (1990): 57-78.

40. Peltier, L. F. "The use of plaster of Paris to fill defects in bone." *Clin. Orthop.* 21 (1961): 1-31.

41. Mackey, D. A. Varlet and D. Debeaumont. "Antibiotic loaded plaster of Paris pellets: an in vitro study of a possible method of load antibiotic therapy in bone infection." *Clin. Orthop.* 167 (1982): 263-268.

42. Yamazaki, Y., S. Oida, Y. Akimoto and S. Shioda. "Response of the mouse femoral muscle to an implant of bone morphogenic protein and plaster of Paris." *Clin. Orthop.* 234 (1988): 240-249.

43. Lin, S. T., S. L. Krebs, S. Kadiyala, K. W. Leong, W. C. LaCourse and B. Kumar. "Development of bioabsorbable glass fibres." *Biomaterials* 15 (1994): 1057-1061.

44. Guo, W., S. Kim, M. D. Grynpas, K. P. H. Pritzker and R. M. Pilliar. "Calcium polyphosphate fibres for composite biomaterials." *The 20th Annual Meeting of the Society for Biomaterials* (1994): 163.

45. Steckel, M. F., F. Ko and A. Skinner. "In vitro mechanical behavior of absorbable composites: CSM short fiber reinforced PDS and PGA." *The 20th Annual Meeting of the Society for Biomaterials* (1994): 193

46. Ibnabddjalil, M., I. H. Loh, C. Chu, N. Blumenthal, H. Alexander and D. Turner. "Effect of surface plasma treatment on the chemical, physical, morphological, and mechanical properties of totally absorbable bone internal fixation devices." *J. Biomed. Mater. Res.* 28 (1994): 289-301.

47. Loh, I. H., H. L. Lin and C. C. Chu. "Plasma surface modification of synthetic absorbable sutures." *J. Appl. Biomater.* 3 (1992): 131-146.

48. Strong, A. B. *Fundamentals for Composite Manufacturing.* Michigan: Society of Manufacturing Engineers, 1989.

49. Jones, R. M. *Mechanics of Composite Materials.* Washington D.C.: Scripta Book Co., 1975.

50. Hyer, M. W. and D. Cohen. "Calculation of stresses in stiffened composite panels." *AIAA Journal* 26 (July '88): 852-857.

51. Fukunaga, H. and H. Sekine. "Optimum design of composite structures for shape, layer angle and layer thickness distributions." *Journal of Composite Materials* 27 (1993): 1479-1492.

52. Willis, J. R. "The overall elastic response of composite materials." *Journal of Applied Mechanics* 50 (December '83): 1202-1209.

53. Eduljee, R. F. and R.L. McCullough. *Elastic Properties of Composites: Continuous Fiber, Particulate, and Discontinuous Fiber*. University of Delaware Center for Composite Materials, Report # 93-07, 1993.

54. Gillespie Jr., J.W. and R.L. McCullough. *SMC Micromechanics Model for Composite Materials: Thermoelastic Properties User's Guide*. Center for Composite Materials, University of Delaware, Report# 87-29, 1987.

55. Whitney, J. M., R. L. McCullough. *University of Delaware Composites Design Guide: Analytic Design Methods*. vol. 2 Delaware: University of Delaware, 1983.

56. McCullough, R. L. *Concepts of Fiber-Resin Composites*. New York: Marcel Dekker, Inc., 1971.

57. Christensen, R. M. *Mechanics of Composite Materials*. New York: John Wiley and Sons, 1979.

58. Lekhnitskii, S. G. *Theory of Elasticity of an Anisotropic Elastic Body*. San Francisco: Holden-Day, Inc., 1963.

59. Wu, C. D. and R. L. McCullough. *Developments in Composite Materials*. London: Applied Science Publishers, 1977.

60. Dreger, D. R. "The challenge of manufacturing composites." *Machine Design* (October 22, 1987): 92-98.

61. Price, A. L. "Composites design and manufacture: one and the same." *Mechanical Engineering* (January '91): 25-28.

62. Ashley, S. "Molding stronger plastic parts." *Mechanical Engineering* (November '93): 56-59.

63. Elegante, T. L. "Filament winding." *Mechanical Engineering* (December '86): 32-36.

64. "Automated filament-winding system creates nonsymmetric composites structures." *Machine Design* (November '86): 18.

65. Sheppard, L. M. "The revolution of filament winding." *Advanced Materials & Processes Incorporating Metal Progress* (July '87): 31-41.

66. English, L. K. "Automated composites fabrication: The Challenge and the Promise." *Mechanical Engineering* (June '88): 45-49.

67. Carlsson, L. A. and R. B. Pipes. *Experimental Characterization of Advanced Composite Materials*. New Jersey: Prentice Hall, 1987.